This dissertation has been
microfilmed exactly as received

66-9578

YOUNG, Dale Travis, 1934-
POWER AND FREQUENCY LIMITATIONS OF GALLIUM ARSENIDE TUNNEL DIODE OSCILLATORS.

The University of Oklahoma, Ph.D., 1966
Engineering, electrical

University Microfilms, Inc., Ann Arbor, Michigan

Downloaded from SHAREOK. Persistent Handle URL: https://hdl.handle.net/11244/2004

THE UNIVERSITY OF OKLAHOMA

GRADUATE COLLEGE

POWER AND FREQUENCY LIMITATIONS OF GALLIUM ARSENIDE TUNNEL DIODE OSCILLATORS

A DISSERTATION

SUBMITTED TO THE GRADUATE FACULTY

in partial fulfillment of the requirements for the

degree of

DOCTOR OF PHILOSOPHY

BY

DALE TRAVIS YOUNG

Norman, Oklahoma

1966

POWER AND FREQUENCY LIMITATIONS OF GALLIUM

ARSENIDE TUNNEL DIODE OSCILLATORS

APPROVED BY

DISSERTATION COMMITTEE

ACKNOWLEDGEMENT

The author is indebted to Professor J. Reynolds and Professor J. D. Palmer for their criticism of the manuscript, to Messrs. C. A. Burrus, S. E. Miller, R. C. Shaw, and W. D. Warters of the Bell Telephone Laboratories for numerous discussions and suggestions.

The author is indebted to the Bell Telephone Laboratories and the University of Oklahoma for financial support.

TABLE OF CONTENTS

		Page
LIST OF TABLES		v
LIST OF ILLUSTRATIONS		vi
Chapter		
I.	INTRODUCTION	1
II.	OBJECTIVES OF THIS INVESTIGATION AND REVIEW OF PREVIOUS WORK	4
III.	THEORY	17
IV.	EXPERIMENTAL PROCEDURE	39
V.	RESULTS AND CONCLUSIONS	71
LIST OF REFERENCES		78

LIST OF TABLES

Table		Page
1.	Experimental Parameters of Low Peak Current Diodes	73

LIST OF ILLUSTRATIONS

Figure		Page
1.	Energy Levels at Zero Bias	6
2.	Volt-Ampere Characteristic for a p-n Junction with Low Doping	7
3.	Volt-Ampere Characteristic for a Backward Diode	7
4.	Volt-Ampere Characteristic for a Tunnel Diode	8
5.	Equivalent Circuit for Tunnel Junction	10
6.	Equivalent Circuit for Tunnel Diode at Accessible Terminals	12
7.	Physical Model for Tunnel Diode	13
8.	Equivalent Circuit and Volt-Ampere Characteristic	18
9.	Possible Biasing Conditions	20
10.	Equivalent Circuit for Experimental Oscillators	23
11.	Low Frequency Equivalent Circuit	24
12.	High Frequency Equivalent Circuit	25
13.	Equivalent Circuit for Analysis	25
14.	Analytical Volt-Ampere Characteristic	26
15.	Equivalent Series and Parallel Circuits	28
16.	Equivalent Circuit Including Resistance	29
17.	Power Efficiency Versus Normalized Frequency	32
18.	Model of Point Contact Tunnel Diode	34

19. Shape of Zinc Strip 41

20. Bias Application for Display 42

21. Circuit for Diode Display 43

22. Low Contact Pressure 44

23. High Contact Pressure 44

24. Correct Contact Pressure 45

25. Pulse Circuit for Low Peak Current Diodes 45

26. Pulse Circuit for High Peak Current Diodes 46

27. X-Band Waveguide Diode Holder 48

28. Impedance of 0.050 Inch X-Band Waveguide 49

29. By-pass Capacitor 50

30. X-Band Wafer Circuit 52

31. X-Band Piston 53

32. Simple X-Band Piston 53

33. Millimeter Waveguide Diode Holder 54

34. Impedance of 0.010 Inch Millimeter Waveguide 56

35. Ridge Waveguide Components 57

36. Millimeter Wafer Circuit 58

37. X-Band Transmission Resonance System 60

38. Oscillator System Block Diagram 62

39. Oscillator Diode Current and Power Output Versus Diode Voltage (Fundamental Oscillation) 63

40. Oscillator Diode Current and Power Output Versus Diode Voltage (Harmonic Output) 65

41. Oscillator Diode Holder with Stabilizing Resistor 66

42. Detector Output Voltage Versus Input Power 68

43. Oscillator Circuit for Life Tests 69

44. Oscillator Power Output Versus Time 70

45. Power Output Limits Versus Frequency 77

POWER AND FREQUENCY LIMITATIONS OF GALLIUM ARSENIDE TUNNEL DIODE OSCILLATORS

CHAPTER I

INTRODUCTION

The discovery in 1958 by L. Esaki (10) of quantum mechanical tunnelling in a forward biased p-n junction provided a simple device with a negative resistance characteristic. This negative resistance effect has been the cause of considerable investigation and research. The Esaki device has exhibited this negative resistance characteristic over a wide range of frequencies and has found considerable application.

This paper is the result of an investigation of GaAs tunnel diodes in waveguide circuits to determine their frequency limitations and obtain small signal, lumped equivalent circuits for these devices when placed in waveguide circuits.

Since the experimental verification of propagating waves in closed tubes by workers at Bell Telephone Laboratories and at the Massachusetts Institute of Technology in 1935, considerable attention has been paid to defining useful low frequency concepts such as voltage, current, and impedance for waveguide circuits. The concept of wave impedance was properly evaluated first by Schelkunoff (22), and a considerable portion of waveguide theory is based on his work. However, even with this outstanding

and very thorough investigation of wave impedance, one is still left with a certain arbitrariness when speaking of the waveguide impedance. There are three different waveguide impedances in common use which are defined in terms of power, voltage, and current of the waveguide mode. The difference between them is a numerical factor with the functional form being the same for all three. These impedances are discussed thoroughly by Southworth (32), and by Montgomery, Purcell, and Dicke (18). Each form of the impedance finds application in different situations. Most situations do not require an absolute number if all parameters can be measured in the waveguide. The measured quantities can all be normalized to the waveguide impedance, and calculations such as return loss, standing wave ratio, et cetera, are independent of the guide impedance. However, for active devices, such as diodes that have some parameters which are more accurately measured outside the waveguide, it is important to know the absolute value of the waveguide impedance in order to relate the device parameters to the waveguide parameters. This allows one to make accurate calculations for active devices which are placed in waveguide circuits. A theoretical calculation of this type was first made by Schelkunoff (23) for a small wire in a reduced height rectangular waveguide, and this calculation was used by DeLoach (8) to characterize diodes.

The purpose of this paper is to determine the frequency and power limitations of GaAs tunnel diode oscillators. This is accomplished by using lumped equivalent circuits for the diodes derived from experimental measurements and theoretical calculations based on the waveguide impedance.

The results of this investigation are the realization experimentally of waveguide circuits for optimum operation of tunnel diode oscillators,

and a theoretical relation for the maximum power available from a tunnel diode oscillator as a function of frequency.

CHAPTER II

OBJECTIVES OF THIS INVESTIGATION AND REVIEW OF PREVIOUS WORK

The general objective of this investigation was to determine the possibility of using tunnel (Esaki) diodes as the primary source of power in an all solid state millimeter waveguide communication system. More specifically, the primary purpose of this investigation was to determine the power and frequency limitations of tunnel diode oscillators both theoretically and experimentally.

The tunnel diode was first introduced and explained theoretically by Esaki (10) in 1958. A number of investigators have used the negative resistance exhibited by this device to operate amplifiers and oscillators over a wide range of frequencies (3, 4, 11, 15, 24, 33, 34, 38).

The theoretical analysis of the tunnel diode has been treated by several authors (6, 10, 14, 21). The paper by Pucel (23) is rather outstanding, and he was one of the first to formulate the now familiar equivalent circuit. The important thing that distinguishes a tunnel diode from the classical p-n junction diode is the quantum mechanical tunnelling of electrons through the junction potential barrier. This mechanism was first proposed by Zener (42) to explain the reverse bias breakdown of semiconductor diodes. However, the mechanism of reverse breakdown in p-n junction diodes is usually the avalanche mechanism (19) except at fairly

low voltages. The magnitude of the breakdown voltage for a p-n junction varies inversely with the doping concentration. The energy level diagrams for a p-n junction with low, medium, and high doping concentrations are shown in Figure 1. Consider the situation where the temperature is at zero degrees absolute so that the Fermi energy level E_f sharply defines the separation between occupied and unoccupied energy states. If an electron is to tunnel across the potential barrier at the depletion layer, it requires an unoccupied energy level across the barrier equal to the energy of the electron. Thus, the p-n junction shown in Figure 1-a will satisfy this requirement only when a large reverse bias is applied, and the junction has the normal volt-ampere characteristic shown in Figure 2. The junction shown in Figure 1-b is the ideal backward diode (9). Here the energy level of the valence band on the p-side is just equal to the energy level of the conduction band on the n-side at zero bias. The application of a reverse bias voltage allows tunnelling in the reverse direction, or electrons from the valence band on the p-side of the barrier can tunnel to the conduction band on the n-side. The volt-ampere characteristic of this junction is shown in Figure 3. This type of junction finds useful application as a low level power detector or frequency converter (5, 9). The junction shown in Figure 1-c allows tunnelling in either the forward or reverse directions. The reverse current is similar to the backward diode. The forward current (electrons tunnelling from the conduction band to the valence band) increases with forward bias voltage until the maximum number of occupied states in the conduction band are opposite unoccupied states in the valence band. Further increase of the bias voltage decreases the current until the

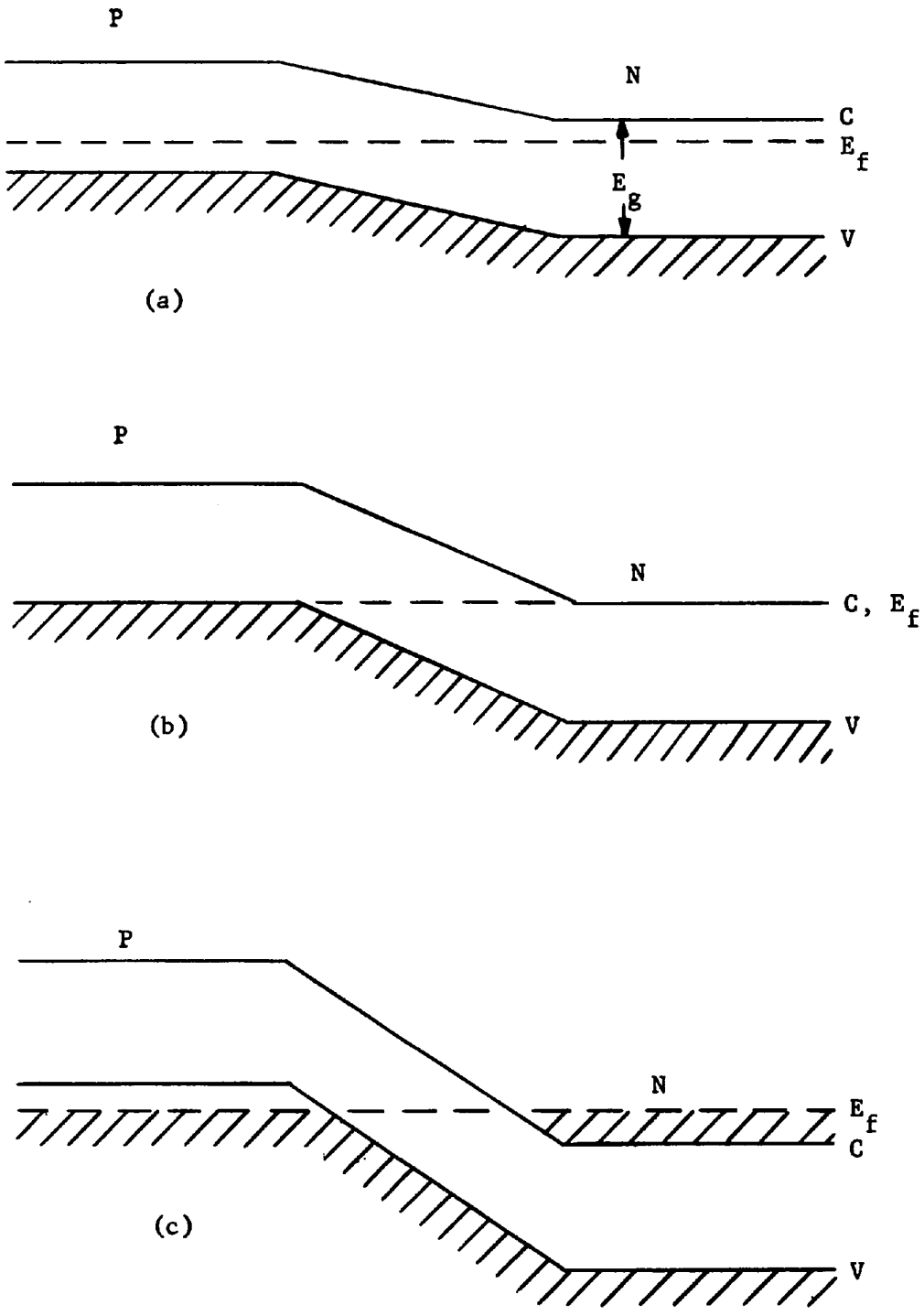

Figure 1 Energy Levels at Zero Bias

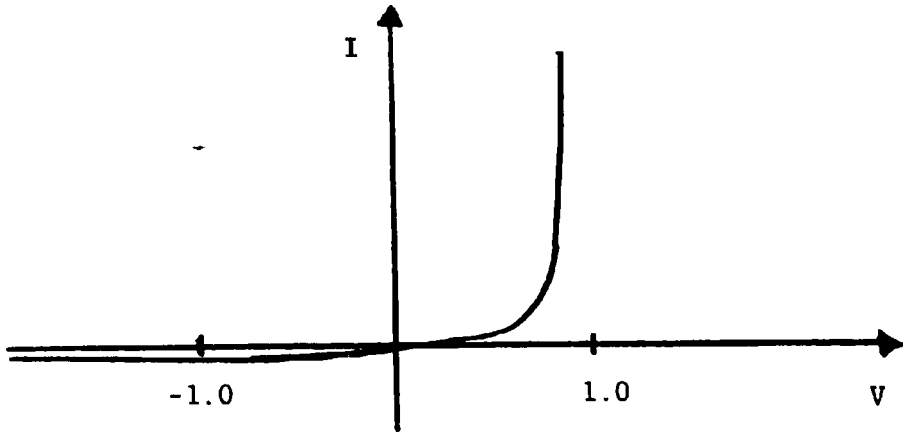

Figure 2 Volt-Ampere Characteristic for a p-n Junction with Low Doping

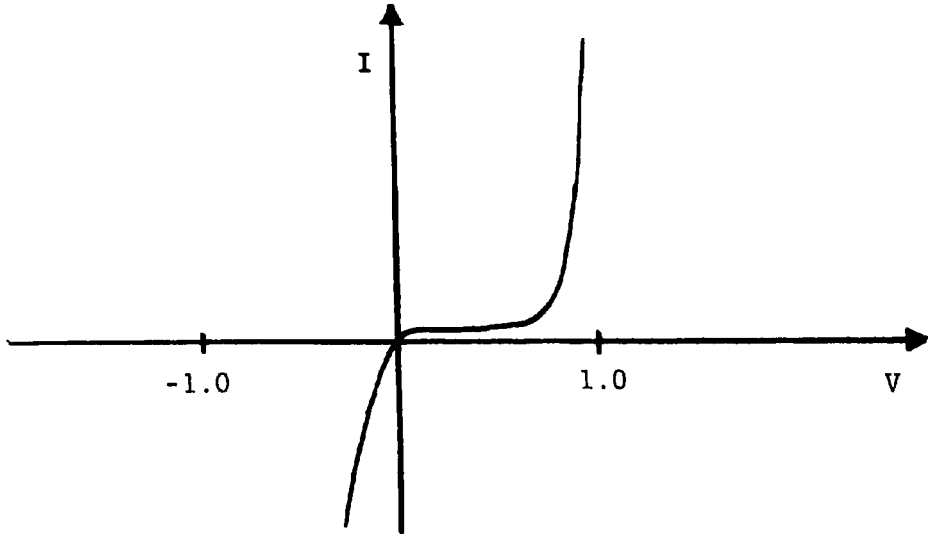

Figure 3 Volt-Ampere Characteristic for a Backward Diode

conduction and valence bands are uncrossed and the tunnelling ceases. The forward current for higher voltage is the normal injection current of a p-n junction. The volt-ampere characteristic for a tunnel diode is

shown in Figure 4. The portion of the characteristic where the current

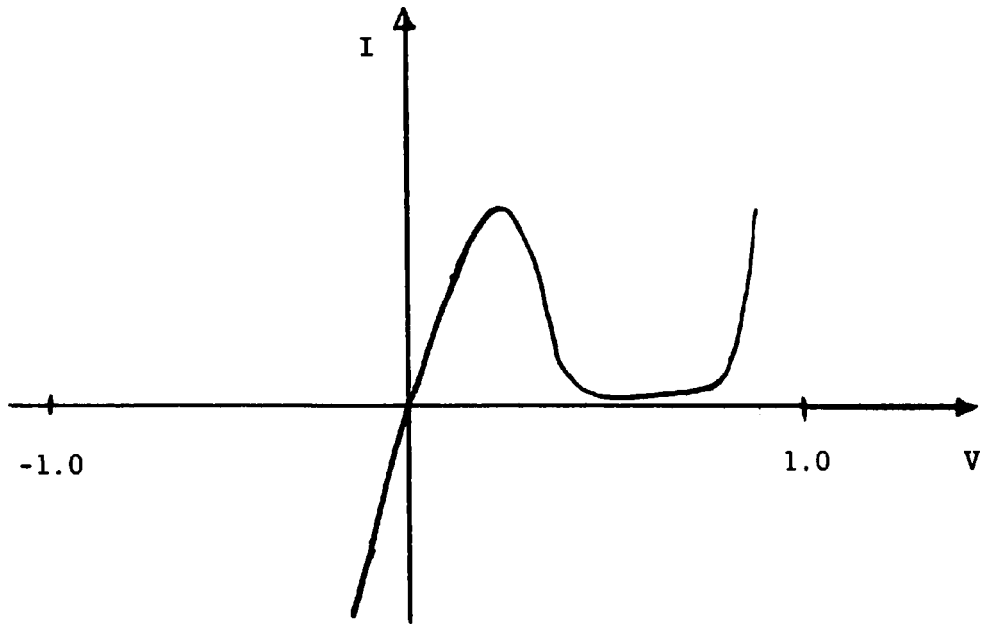

Figure 4 Volt-Ampere Characteristic for a Tunnel Diode

decreases when the voltage increases is responsible for the negative resistance effect, which is the most useful property of a tunnel diode.

Qualitative calculations for a degenerate p-n junction (tunnel diode) are difficult even at zero degrees absolute (14). A reasonable approximation of the depletion layer thickness can be obtained from the simple model calculated by Lesk, et al. (16). They assume a simple triangular energy barrier, which amounts to a constant electric field in the barrier region and use the WKB technique to calculate the tunnelling probability per second through the barrier.

$$w = \frac{aeF}{h} \exp\left(\frac{-4}{3} (2 m_{eff})^{1/2} \frac{E_g^{3/2}}{\hbar eF} \right) \text{ tunnelling probability/second} \quad (2\text{-}1)$$

where a is the lattice constant

e is the electron charge

F is the electric field intensity

h is Planck's constant

m_{eff} is the effective mass of an electron in the semiconductor

E_g is the energy gap.

If one calculates w as a function of F, an extremely sharp increase in w is found when F is in the vicinity of 10^8 volts per meter. This requires that the junction width for this model be:

$$W = \frac{E_g}{10^8} \approx 135 \text{ A}^{\circ} \qquad (2\text{-}2)$$

This establishes the order of magnitude of the depletion layer thickness.

Chynoweth (6) estimates that the electrons tunnel at the velocity of light, which would require a transit time across the barrier of approximately 10^{-16} seconds. The tunnelling of an electron from the valence band on the p-side of the junction across the depletion layer to the conduction band on the n-side causes a charge imbalance, which must be balanced by a redistribution of the majority carriers on both sides of the junction. The time required for the redistribution of charge is characterized by the familiar dielectric relaxation time of a conducting medium (31).

$$\tau = \epsilon/\sigma \qquad (2\text{-}3)$$

where

$$\epsilon = 97.7 \times 10^{-2} \text{ farads/meter}$$

$$\frac{1}{\sigma} = 10^{-5} \text{ ohm-meter.}$$

This means a relaxation time of about 10^{-15} seconds for the highly doped

GaAs used in this experiment, and therefore, no changes in the tunnelling current for sinusoidally varying voltages from the dc characteristic for frequencies below 10^{15} c/s are expected. The next consideration is the effect of diffusion. The diffusion current is practically zero in the tunnelling region, and the conductance and capacitance due to diffusion (17) are neglected.

The difference between the diode voltages where the peak and valley current occur varies directly with the energy gap of the semiconductor. GaAs has the largest differential voltage of the materials from which useful tunnel diodes can be made. This voltage is fairly constant for a wide range of peak current diodes made from the same material.

The final consideration of the junction is the depletion layer capacitance. The capacitance can be calculated from Poisson's equation, assuming an abrupt p-n junction (19). This capacitance is large due to the thinness of the barrier and is voltage dependent, but is independent of frequency. A small signal equivalent circuit for the tunnel junction consisting of a parallel conductance and capacitance, which is practically frequency independent, is shown in Figure 5. The value of G or R_-

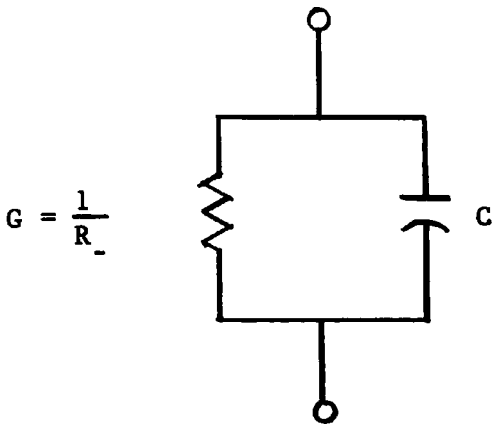

Figure 5 Equivalent Circuit for Tunnel Junction

for a particular operating point is determined from the slope of the volt-ampere characteristic. The capacitance can be calculated from the following formula:

$$C = \frac{\epsilon A}{W} \qquad (2\text{-}4)$$

where A is the junction area

W is the depletion layer thickness.

The resistance of the junction is inversely proportional to the product JA, where J is the current density and A is the junction area. The capacitance will vary as A/W, so that the time constant of the junction will be independent of the area, and will vary as $(JW)^{-1}$. Thus, high frequency performance requires the product JW to be large. However, J decreases very rapidly with W for a given material, so that the highest value for this product is generally obtained for the thinnest junctions.

If the junction itself were accessible, then the diode could be made to oscillate at any frequency, provided a small enough inductance could be resonated with the capacitance. However, the present state-of-the-art has not produced thin enough semiconductor chips with contacts, so that a third element must be added to the equivalent circuit. This element is a positive parasitic resistance, and the complete equivalent circuit is shown in Figure 6. The circuit now has a definite frequency limitation. This frequency limit is called the resistive cutoff frequency, and it is the frequency where the resistance between the accessible terminals goes to zero. This frequency is given by the following formula:

$$f_c = \frac{1}{2\pi R_L C}\left(\frac{R_-}{r_s} - 1\right)^{1/2} . \qquad (2\text{-}5)$$

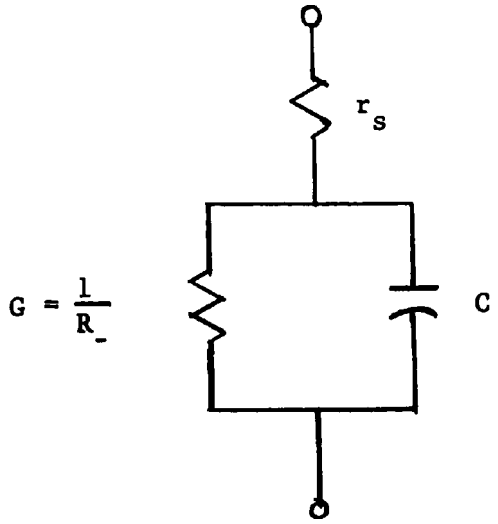

Figure 6 Equivalent Circuit for Tunnel Diode at Accessible Terminals

It is necessary to examine at this point the geometry of the diode. If the diode is a cylinder, then the parasitic resistance (r_s) is proportional to the length of the semiconductor divided by the area of the junction. The cutoff frequency is independent of the area, and it is limited by the height of the cylinder. However, if the familiar point contact geometry is used, the resistance (r_s) is inversely proportional to the square root of the area, and the cutoff frequency is now approximately proportional to the inverse fourth root of the area:

$$f_c \propto \frac{1}{A^{1/4}} \qquad (2\text{-}6)$$

for $\frac{R_-}{r_s} \gg 1$.

The cutoff frequency may be increased by decreasing the area. Unfortunately, the spreading resistance is not completely independent of frequency. Hines (12) has used the following model to calculate the parasitic resistance, which considers the frequency dependent resistance due to skin effect. The geometry of the model is shown in Figure 7. For

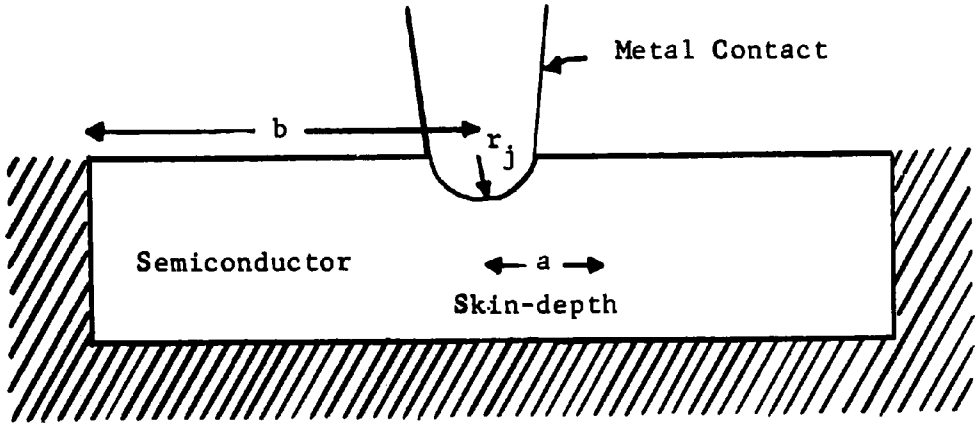

Figure 7 Physical Model for Tunnel Diode

the region near the junction, the spreading resistance is taken as though the outer boundary were at infinity, and the skin resistance for the region beyond a radius equal to one "skin-depth" is added. This results in the following formula:

$$r_s = \frac{\rho}{2\pi r_j} + \frac{\rho_s}{2\pi} \ln \frac{b}{a} \qquad (2\text{-}7)$$

where ρ is the bulk resistivity

ρ_s is the skin resistance.

The second term of equation (2-7) varies as the square root of frequency. While the value of the second term is small in most cases of interest, it can be appreciable at frequencies near 100 Gc, and it cannot always be neglected.

Oguey (22) has made an analysis of high frequency performance of tunnel diodes, which is comprehensive on the capabilities of the diodes themselves with respect to material considerations. However, he used very idealized circuit models, and this investigation offers experimentally realized power outputs in simple, practical circuits, which should be more realistic. Higher resistive qutoff frequencies are realizable for a given peak current with n-type GaAs and the point contact geometry. This is due primarily to the high mobility in the n-type material and the consequent lower parasitic resistance.

An important part of this investigation is the measurement of the diode equivalent circuits, using the transmission resonance technique of DeLoach (8). DeLoach recognized that the diode equivalent circuit parameters r_s and C could be measured at high frequencies in a waveguide if the proper value for the waveguide impedance could be chosen. The theoretical basis for choosing this impedance is an approximate calculation by Schelkunoff (23) of the radiation impedance seen by a short, thin wire across the narrow dimension of a rectangular waveguide. The value of guide impedance is:

$$Z_g = 754 \frac{b}{a} \frac{\lambda_g}{\lambda} \sin \frac{\pi d}{a} \text{ ohms} \qquad (2\text{-}8)$$

where b is the guide height

a is the guide width

λ_g is the guide wavelength

λ is the free space wavelength

d is the distance of the wire from the side wall.

Slater (29) obtains the same impedance by calculating the radiation impedance for an electric dipole in a waveguide. This determines the limits of approximation involved in Schelkunoff's calculation, and it necessitates reducing the height of a standard height guide to obtain accurate experimental results. DeLoach obtained the following formulae for diode parameters in a reduced height guide with the diode at the center of the guide:

$$r_s = \frac{Z_g}{2} \frac{1}{T^{1/2} - 1} \tag{2-9}$$

$$C = \frac{1}{\pi Z_g} \frac{f_1 - f_2}{f_1 f_2} (T^{1/2} - 1)(1 - \frac{2}{T})^{1/2} \tag{2-10}$$

where T is the power transmission loss ratio at resonance

f_1 and f_2 are the upper and lower 3dB frequencies.

As a further check on the experimental results, DeLoach measured the capacitance of the same diodes on a low frequency bridge, and he obtained the same capacitance values as those given by the waveguide measurement, which was a strong validation of the theory.

The point of departure for the experimental work of this investigation is the work of Burrus (4) on GaAs tunnel diodes. Burrus obtained fundamental oscillations from n-type GaAs in reduced height RG99/U waveguide in the frequency range of 50 Gc/s to 100 Gc/s. Burrus used only the simplest waveguide circuit, and the output power he obtained was far below the theoretical maximum first obtained by Trambarulo (35), and verified experimentally by Kim and Brandli (15) at a frequency of 2 Gc/s in a strip line circuit. This theoretical limit was also verified

by Schneider (24) in strip line circuits at 5 Gc/s to 7 Gc/s. The work here is the first to obtain this optimum experimentally using waveguide circuits at 10 Gc/s and 50 Gc/s.

CHAPTER III

THEORY

The theoretical determination of the output power available from a tunnel diode oscillator begins from the equivalent circuit model and the volt-ampere characteristic shown in Figure 8. The equivalent circuit shown represents the simplest possible oscillator circuit for a tunnel diode. The terminals AB represent the accessible terminals of the tunnel diode, and these parameters are fixed once a diode is selected. The parameters R and L are adjustable, although they may include the parasitic elements of a practical circuit. These parameters often cannot be reduced to zero, and this will limit the magnitude of the peak current of the tunnel diode for desirable operation in certain circuits, as shall be seen later. The source E is considered to be an ideal voltage source which is independent of the current i, and constant with time. In the solution of the equations for the circuit, there are two degrees of freedom or two independent variables. The most convenient pair of equations are the following:

$$E = i_1 R + L \frac{di_1}{dt} + e_r \tag{3-1}$$

$$i_1 = C \frac{de_r}{dt} + f(e_r) \ . \tag{3-2}$$

Rearranging these equations, one obtains:

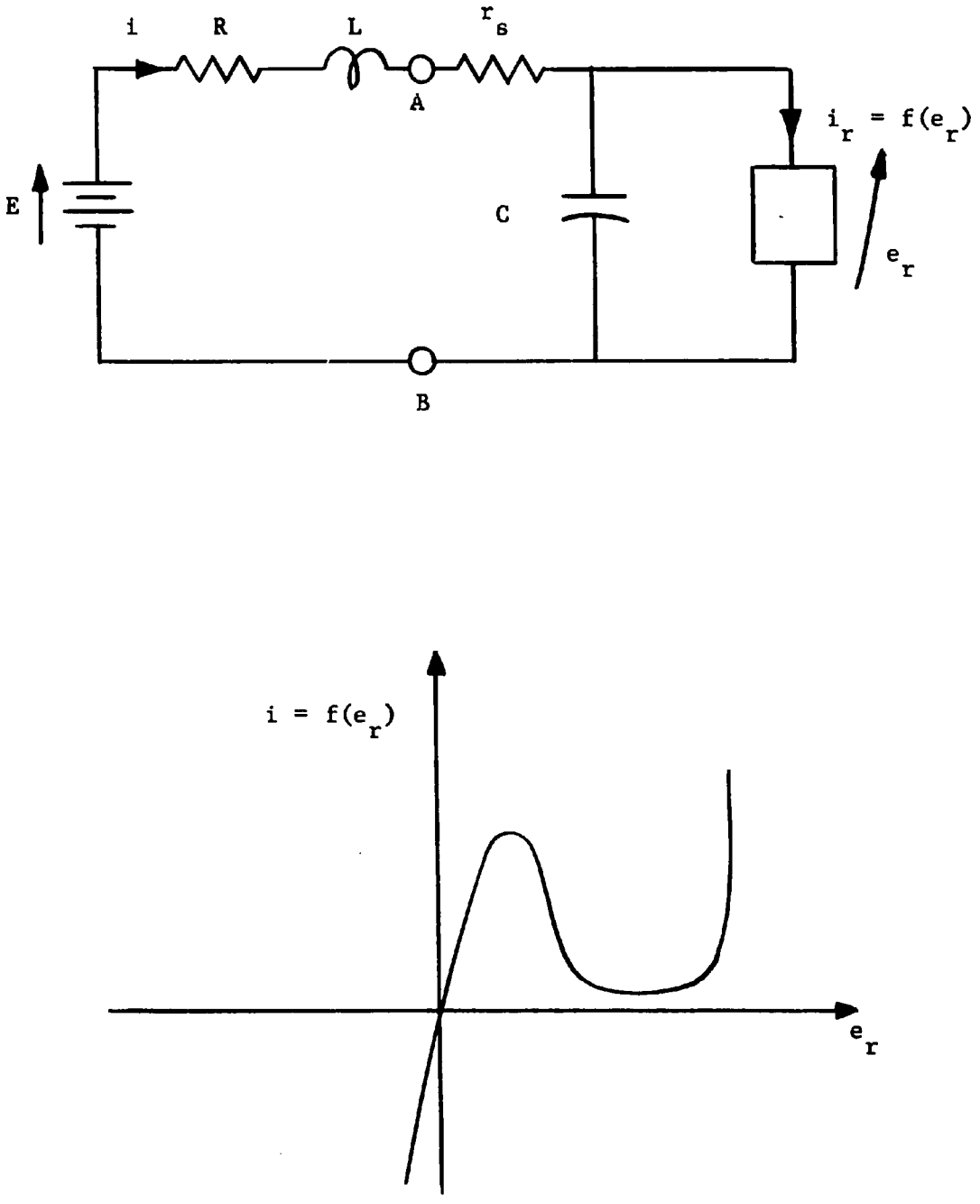

Figure 8 Equivalent Circuit and Volt-Ampere Characteristic

$$\frac{di_l}{dt} = \frac{E}{L} - i_l \frac{R}{L} - \frac{e_r}{L} \tag{3-1}$$

$$\frac{de_r}{dt} = \frac{i_l}{C} - \frac{f(e_r)}{C} \quad . \tag{3-2}$$

In examining the equilibrium solutions of these equations it can be seen that

$$\frac{di_l}{dt} = \frac{de_r}{dt} = 0 \tag{3-3}$$

is required. Then $i = i_r$ and (3-1) can be solved by placing the familiar dc load line on the volt-ampere characteristic for the tunnel diode. For a particular diode this may have several possibilities, as the three shown in Figure 9.

The situation in Figure 9-a is of little practical interest. Figure 9-b is a case of considerable interest (28). There are three points of equilibrium. The points 1 and 3 are stable points and point 2 is unstable. It is possible to switch the diode from state 1 to 3, or from 3 to 1, with the application of a pulse, and the device can be used as a bistable switch. Figure 9-c is the case of most interest, and the equilibrium point will be examined in detail. One can apply a small signal analysis to this case about the equilibrium point with coordinates (E_o, I_o). One can obtain linear soluble equations if $f(e_r)$ is expanded in a Taylor's series about the point (E_o, I_o), and only the first order term is retained.

$$f(e_r) \approx f(E_o) + \frac{df(E_o)}{de_r} (e_r - E_o) \tag{3-4}$$

Using this approximation in (3-2) one obtains:

$$\frac{di_l}{dt} = \frac{E}{L} - i_l \frac{R}{L} - \frac{1}{L} e_r \tag{3-5}$$

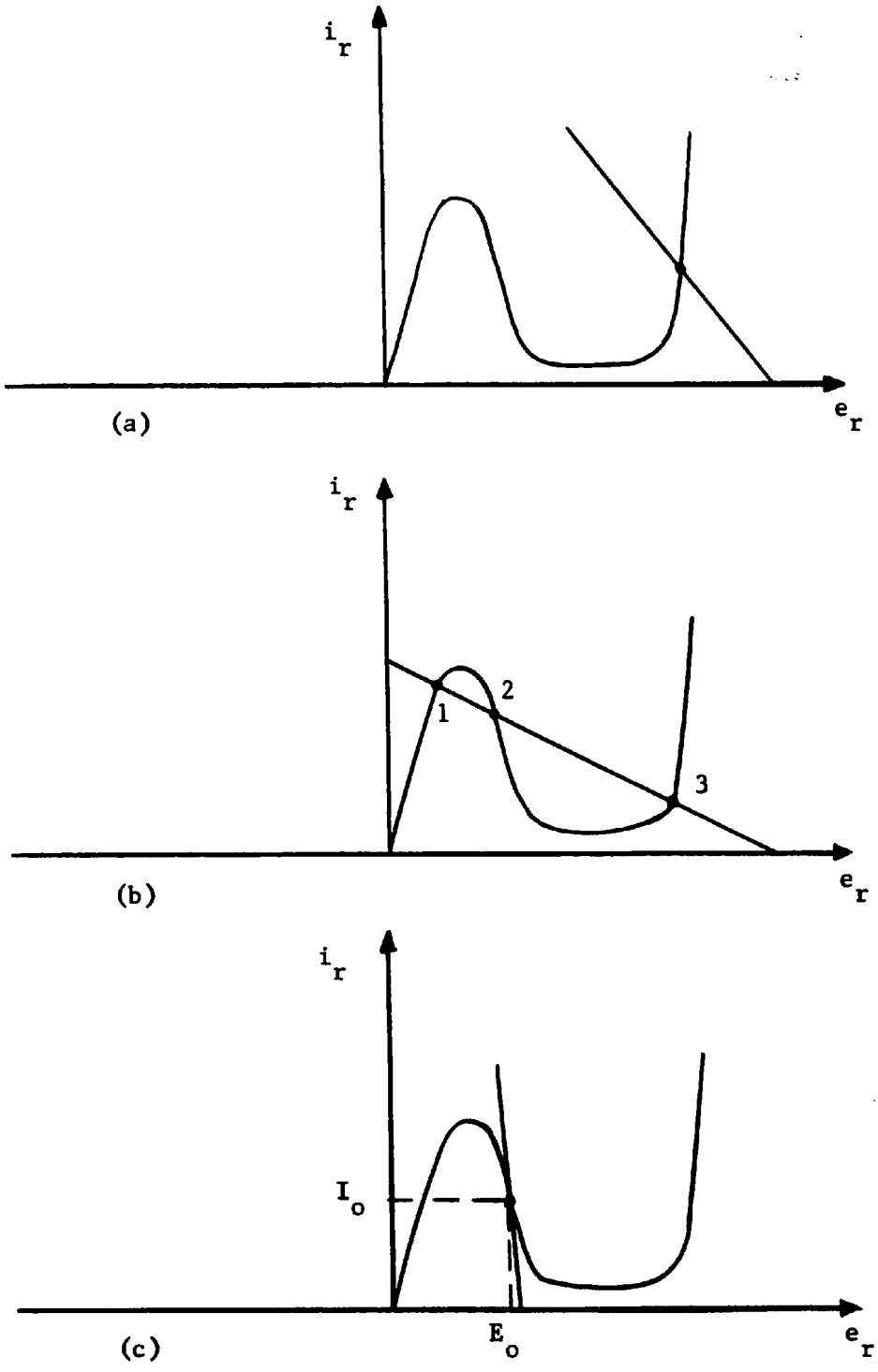

Figure 9 Possible Biasing Conditions

$$\frac{de_r}{dt} = \frac{i_1}{C} - \frac{1}{C}\left[I_o + g(e_r - E_o)\right] \qquad (3\text{-}6)$$

where $g = \dfrac{df(E_o)}{de_r}$.

Equations (3-5) and (3-6) are simultaneous differential equations with constant coefficients. The quantities of real interest are the deviations from the equilibrium point $(e_r - E_o)$ and $(i_1 - I_o)$. Letting

$$e = e_r - E_o \qquad (3\text{-}7)$$

$$i = i_1 - I_o \qquad (3\text{-}8)$$

(3-5) and (3-6) can be written as:

$$\frac{di}{dt} = -\frac{R}{L} i - \frac{1}{L} e \qquad (3\text{-}9)$$

$$\frac{de}{dt} = \frac{i}{C} - \frac{g}{C} e \; . \qquad (3\text{-}10)$$

The solution of (3-9) and (3-10) are exponential functions of time with the following characteristic values:

$$\lambda_{1,2} = \frac{1}{2}\left\{ -\left(\frac{g}{C} + \frac{R}{L}\right) \pm \left[\left(\frac{g}{C} + \frac{R}{L}\right)^2 + \frac{4}{LC}\left(-1 - Rg\right)\right]^{1/2}\right\}. \qquad (3\text{-}11)$$

These solutions are stable only if the real parts of $\lambda_{1,2}$ are negative. Hines (12) has made a rather thorough analysis of the equation, and by using the following substitutions, obtains a two parameter equation.

Let $\omega_o = \dfrac{1}{(LC)^{1/2}}$ and $Q_- = \omega_o CR_-$,

then the expression for $\lambda_{1,2}$ can be written as:

$$\frac{\lambda_{1,2}}{\omega_o} = \frac{1}{2Q_-}\left(1 - \frac{R}{R_-} Q_-^2\right) \pm j\left[\left(1 - \frac{R}{R_-}\right) - \frac{1}{4Q_-^2}\left(1 - \frac{RQ_-^2}{R_-}\right)^2\right]^{1/2} . \qquad (3\text{-}12)$$

Hines' numerical analysis gives the following important requirements for stability in terms of Q_-. It is not possible to stabilize the circuit

if Q_- is less than 1 by adjusting the ratio R/R_-. The case of interest in these experiments is when Q_- is greater than 1, then the requirements for stability are

$$\frac{1}{Q_-^2} < \frac{R}{R_-} < 1 \tag{3-13}$$

or

$$L\omega_d < R < R_- \tag{3-14}$$

where $\omega_d = \frac{1}{R_-C}$ is a characteristic frequency, which is a constant for a fixed material. This is true since C will be the diode junction capacitance in these experiments. Equation (3-14) is important because in all the circuits investigated the minimum value of parasitic inductance always limited the magnitude of the peak current of the diodes. Above a certain peak current the diodes could not be stabilized in the circuit since R_- is inversely proportional to the peak current. This in turn limits the power available from a particular circuit. Further investigation of (3-14) reveals the type of instability if the inequalities are not satisfied. If R is not less than R_-, one has growing exponential solutions for (3-9) and (3-10). The result in the practical sense is a relaxation oscillation. If R is less than R_-, but not greater than $L\omega_d$, then growing sinusoidal solutions result. These sinusoidal oscillations occur in the high frequency part of the circuit. A more complex circuit, which represents the actual physical circuits used in these experiments, is shown in Figure 10. The elements to the right of the section AA' represent the diode. The variable elements Z_g and L_g represent the high frequency part of the circuit contributed by a waveguide operating above its cutoff frequency with a tuning element,

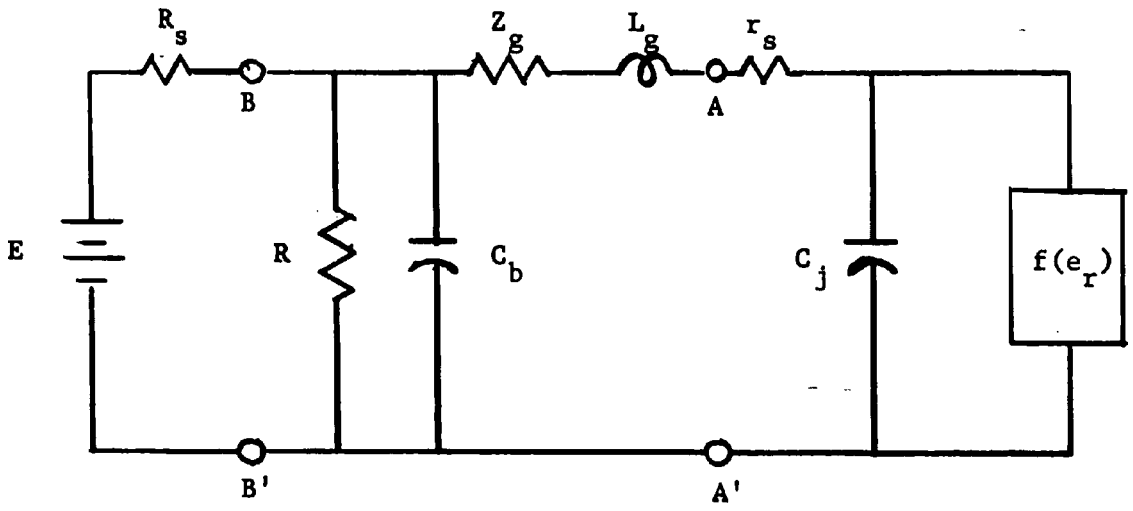

Figure 10 Equivalent Circuit for Experimental Oscillators

such as a movable short-circuiting piston, and these parameters are functions of frequency. The capacitance C_b is a by-pass capacitance, which is practically a short circuit at the waveguide frequencies, but allows dc bias from the bias circuit to the left of the section BB' to bias the tunnel diode in the negative resistance region. The element R is a stabilizing resistor to suppress oscillations in the bias circuit, since the by-pass capacitor begins to act like an open circuit below a frequency of 100 Mc/s. R is one of the critical elements in the practical operation of a tunnel diode as a high frequency oscillator. At frequencies below the waveguide cutoff, the circuit in the preceding Figure 10 becomes the circuit shown in Figure 11. Here L_m is the inductance due to the waveguide and other circuits. It is a parasitic inductance which cannot be reduced without changing the waveguide circuitry. Here it is

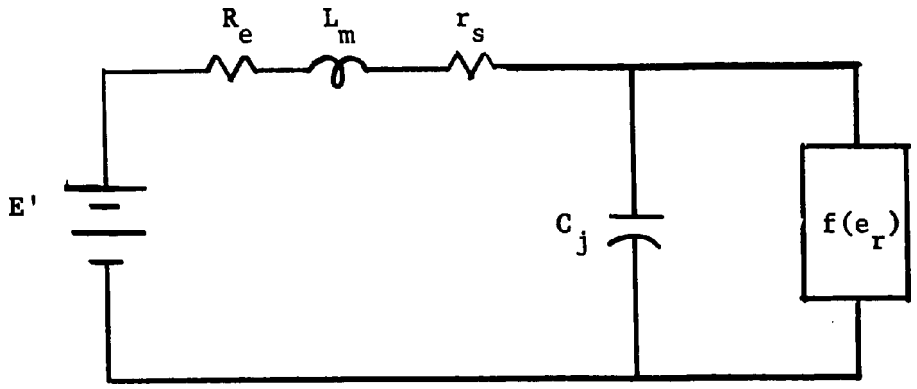

Figure 11 Low Frequency Equivalent Circuit

imperative for proper operation of the diode oscillator at the high frequencies, that the diode is absolutely stable in the low frequency circuit. This requires:

$$L_m \omega_d < R_e + r_s < R_- \quad . \tag{3-15}$$

If $R_e + r_s$ is greater than R_-, switching takes place in the bias circuit, and high frequency oscillation is impossible. If $R_e + r_s$ is less than $L\omega_d$, then low frequency sinusoidal oscillations occur in the bias circuit, and a part of the maximum power available from the diode as an oscillator is not available in the waveguide circuit, which is the desired circuit for oscillations. Although simultaneous oscillations in the bias circuit and the waveguide circuit are possible, this situation is far from optimum, and is to be avoided in practical circuits. Since L_m is the total parasitic inductance, which includes the inductance of leads, it is necessary to locate R_e as close to the diode as is physically possible to stabilize the larger peak current diodes. However,

it is not feasible to locate R_e inside the waveguide itself. A minimum parasitic inductance still exists for a particular waveguide circuit, which limits the peak current of the diodes for that circuit.

A topic of considerable interest is the maximum power available from a tunnel diode oscillator. The circuit of interest for this computation is the high frequency part of the circuit in Figure 10 with the by-pass capacitor C_b acting as a short circuit.

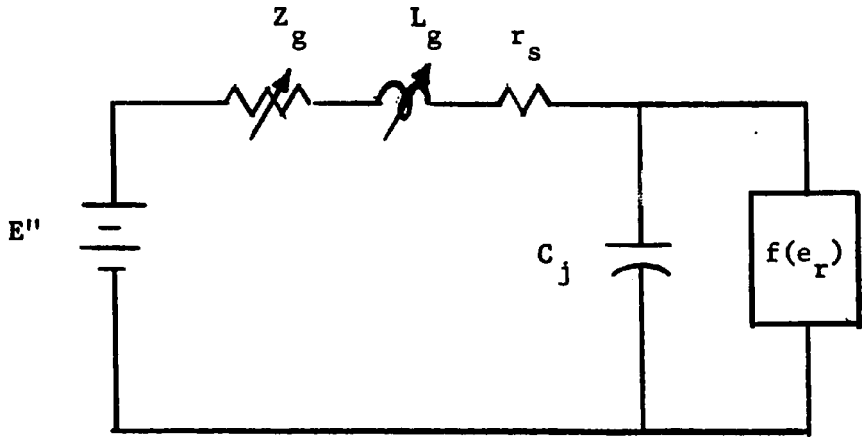

Figure 12 High Frequency Equivalent Circuit

The analysis is simplified if Z_g and r_s are lumped into an equivalent resistance R, and the subscripts are dropped from the other parameters, and the circuit shown in Figure 13 is considered.

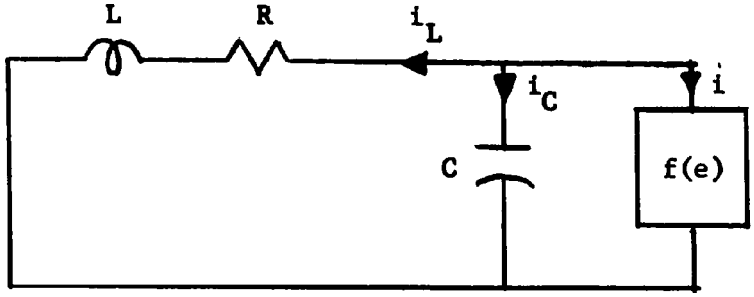

Figure 13 Equivalent Circuit for Analysis

This circuit is identical to a negative resistance oscillator analyzed by Cunningham (7). The analysis is also similar to an analysis of Kim and Brandli (15). The first step in the analysis is to obtain an analytical expression for the tunnel diode characteristic. One is primarily interested in biasing the tunnel diode at the voltage where the negative resistance is a maximum. The quantities of interest are the time varying voltage and current about this bias point, as in the case of the previously discussed stability conditions. A reasonable approximation to the diode characteristic about the point of maximum negative resistance is obtained from a symmetrical third order curve. This curve is made to fit the actual characteristic at the peak and valley currents. The analytical expression is:

$$i = -ae + be^3 \tag{3-16}$$

and a sketch is shown in Figure 14.

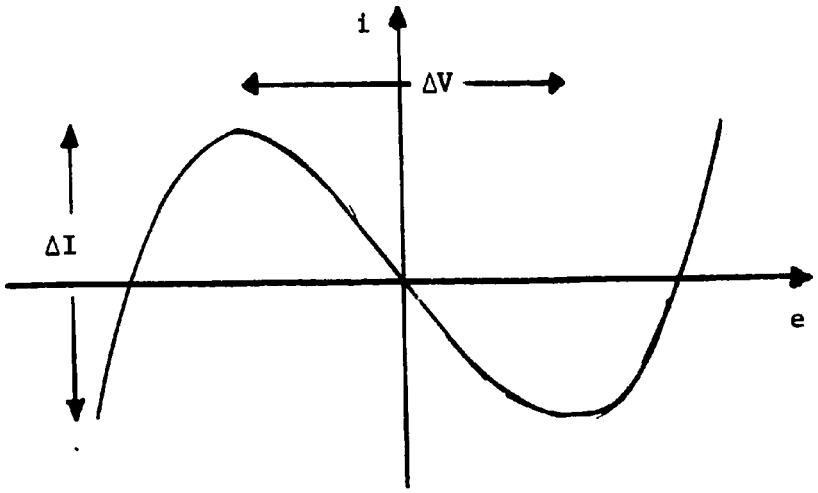

Figure 14 Analytical Volt-Ampere Characteristic

This requires that the constants a and b have the following values in terms of ΔV and ΔI which are parameters of the diodes. These parameters are easily measured from a 60 c/s trace on an oscilloscope.

$$a = \frac{3}{2}\frac{\Delta I}{\Delta V} \tag{3-17}$$

$$b = 2\frac{\Delta I}{\Delta V^3} \tag{3-18}$$

However, the analysis is carried through in terms of a and b, and (3-17) and (3-18) will be used later. Referring to Figure 13, one has:

$$i_L + i_C + i = 0 \tag{3-19}$$

where $i_C = C\frac{de}{dt}$, $i = -ae + be^3$, and $L\frac{di_L}{dt} + Ri_L = e$.

The inclusion of the resistance R in the analysis at this point causes considerable complication. For the present, assume the voltage across the resistance can be neglected in comparison with the voltage across the inductance, and the effect of this resistance will be examined later. Making this approximation, (3-19) becomes:

$$\ddot{e} - \frac{a}{C}\left(1 - \frac{3b}{a}e^2\right)\dot{e} + \frac{1}{LC}e = 0 \tag{3-20}$$

where

$$\dot{e} = \frac{de}{dt}, \quad \ddot{e} = \frac{d^2e}{dt^2}$$

or letting $\omega_o^2 = \frac{1}{LC}$, $\beta = \frac{3b}{a}$, and $\alpha = \frac{a}{C\omega_o}$ one has

$$\ddot{e} - \alpha(1 - \beta e^2)\omega_o\dot{e} + \omega_o^2 e = 0. \tag{3-21}$$

If it is assumed that the value of α is small, then a perturbation solution of second order in α can be shown to be (7):

$$e = E\cos\omega t + \alpha\frac{E}{8}(3\sin\omega t - \sin 3\omega t) \tag{3-22}$$
$$- \alpha^2\frac{E}{192}(13\cos\omega t - 18\cos 3\omega t + 5\cos 5\omega t)$$

where

$$\omega = \frac{\omega_o}{1 + \alpha^2/16}$$

$$E = \pm \frac{2}{\beta^{1/2}} = \pm \Delta V \ .$$

The fundamental frequency is the term of interest, and the peak amplitude is:

$$E_p = \Delta V \left[1 + \left(\frac{3\alpha}{8}\right)^2\right]^{1/2} \approx \Delta V \ . \qquad (3\text{-}23)$$

The effect of the neglected resistance may be accounted for in the following way. Since the oscillation is practically a pure sinusoid for small values of α, the series resistance inductance may be considered as an equivalent parallel combination at the resonant frequency. The circuits shown in Figure 15 are equivalent at the angular frequency ω_o if

$$G' = \frac{R}{R^2 + \omega_o^2 L^2} \qquad \text{and} \qquad \frac{1}{L'} = \frac{\omega_o^2 L}{R^2 + \omega_o^2 L^2} \ .$$

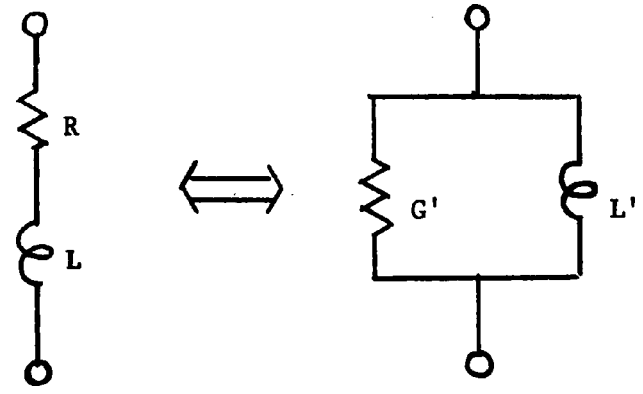

Figure 15 Equivalent Series and Parallel Circuits

Since $\omega_o L \gg R$ these relations are approximately given by:

$$G' \approx \frac{RC}{L} \qquad \text{and} \qquad L' \approx L \,. \tag{3-24}$$

This leads to the equivalent circuit shown in Figure 16.

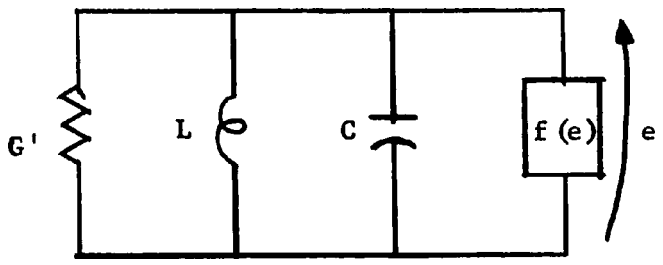

Figure 16 Equivalent Circuit Including Resistance

Now G' can be combined with the resistance of the diode and the only change in the preceding analysis is replacement of the parameter a by an a' where:

$$a' = a - G' = a - \frac{RC}{L} \,. \tag{3-25}$$

This allows some observations about the power dissipated in R.

$$P = \frac{E'^2 G'}{2} \tag{3-26}$$

where

$$E' = 2\left(\frac{a'}{3b}\right)^{1/2}$$

then (3-26) becomes:

$$P = \frac{2}{3b}\left(a - G'\right) G' \,. \tag{3-27}$$

If the power is considered as a function of G', one can determine the value of G' which makes the power a maximum.

$$\frac{dP}{dG'} = 0 = \frac{2}{3b}(a - G') - \frac{2}{3b} G' \tag{3-28}$$

which requires:

$$G' = \frac{a}{2} \tag{3-29}$$

Substituting this value into (3-27), and using (3-17) and (3-18), one obtains Kim and Brandli's result (15):

$$P_m = \frac{3}{16} \Delta V \, \Delta I \, . \tag{3-30}$$

The important result of the maximum frequency for maximum power generation from a diode can be obtained by remembering that the minimum value of the resistance R is the spreading resistance of the diode r_s. This determines the minimum inductance L necessary to satisfy the maximum power condition from (3-29) as

$$\frac{r_s C}{L_{min}} = \frac{1}{2R_-} \tag{3-31}$$

or

$$L_m = 2R_- \, r_s C \tag{3-32}$$

which determines the frequency ω_{max}

$$\omega_{max} = \frac{1}{(L_m C)^{1/2}} = \frac{1}{C(2r_s R_-)^{1/2}} \, . \tag{3-33}$$

Recalling the equation for the diode cutoff frequency from the previous chapter, equation (2-5), and utilizing the fact that for diodes of interest $R_-/r_s \gg 1$, the cutoff frequency ω_c is approximately:

$$\omega_c \approx \frac{1}{C(r_s \, R_-)^{1/2}} \, . \tag{3-34}$$

Comparing (3-33) and (3-34) it can be seen that:

$$\omega_c = 2^{1/2} \, \omega_{max} \, . \tag{3-35}$$

This is equivalent to the result of Kim and Brandli (15). Equation (3-35) is an important result, since it provides an important figure of merit for tunnel diodes by defining the frequency limit for significant power generation. Continuing this point, one can obtain an equation for the power available for useful output power at frequencies below this maximum, since the total power generated at the maximum frequency is dissipated in the diode itself, and is of no value. The resistance R can be considered to be the sum of a load resistor R_e, and the diode spreading resistance r_s, and the ratio of the power delivered to the load to the total power available is:

$$\eta = \frac{P_e}{P_a} = \frac{R_e}{R_e + r_s} = 1 - \frac{r_s}{R} . \qquad (3\text{-}36)$$

Now if it is required that R satisfies the optimum power condition, (3-31) yields

$$\eta = 1 - \frac{2 r_s R_- C}{L} . \qquad (3\text{-}37)$$

Replacing L by $\frac{1}{\omega^2 C}$ one obtains

$$\eta = 1 - \left(\frac{\omega}{\omega_{max}}\right)^2 \quad \text{for} \quad \omega < \omega_{max} . \qquad (3\text{-}38)$$

Since $\omega_c = 2^{1/2} \omega_{max}$ then

$$\eta = 1 - \frac{2\omega^2}{\omega_c^2} . \qquad (3\text{-}39)$$

Equation (3-39) gives a practical limit for the expected maximum power available for a tunnel diode oscillator. Equation (3-39) is plotted in Figure 17, and it can be seen that obtaining the maximum theoretical power available from a tunnel diode requires that the operating frequency be considerably below the resistive cutoff frequency.

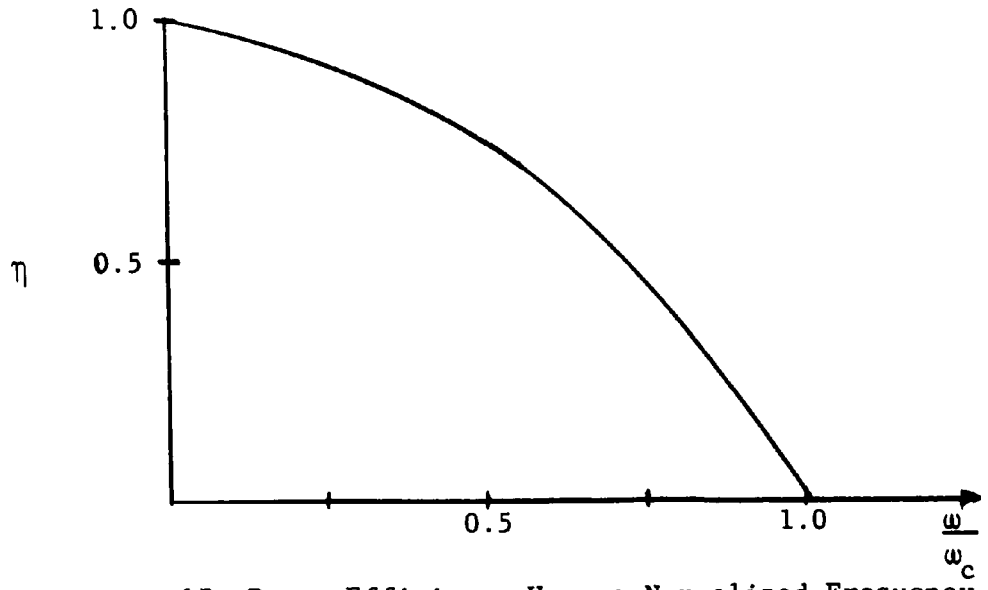

Figure 17 Power Efficiency Versus Normalized Frequency

Finally, the maximum frequency for any oscillation to exist can be determined from the expression $E' = 2\left(\frac{a'}{3b}\right)^{1/2}$. This occurs when a' becomes zero and hence $E = 0$. This occurs when $R = r_s$ and $L = r_s R_- C$, and therefore, the maximum frequency of oscillation is:

$$\omega = \frac{1}{C(r_s R_-)^{1/2}} \quad . \tag{3-40}$$

This is approximately equal to the resistive cutoff frequency defined previously. It is also interesting to compute the voltage swing under the conditions of maximum power generation.

$$E_p \approx \frac{\Delta V}{2^{1/2}} \tag{3-41}$$

Thus the voltage swing is somewhat smaller when the output is optimum, which should be an advantage from the standpoint of degradation, although the experimental results show that degradation for the n-type GaAs tunnel diodes is so serious that practical oscillator circuits are not possible

at the present time using this material.

It is now possible to return to the physics of the tunnel diode, and correlate the circuit limitations on the tunnel diode oscillators with the physics of the material. The point contact tunnel diodes used in these experiments are believed to be similar to alloy junction diodes (36). The chip of semiconductor material is heavily doped with one type of doping, and then an extremely light pressure contact is made with a metal whisker, which contains the opposite doping to the base material doping. The tunnel diode junction is then formed by passing a relatively large pulse of current through the metal semiconductor pressure contact. This causes the region near the junction to melt, and the original doping of the base semiconductor near the junction is compensated by the material of the metal whisker. The result is believed to be similar to an alloyed p-n junction with the junction established in the vicinity of the original junction, as shown in Figure 18. The model shown in Figure 18 is rather idealized with the metal semiconductor contact shown as a hemispherical contact, and it is entirely possible that the actual metal-semiconductor contact is more nearly flat. However, it is reasonably certain that the shape of the contact lies somewhere between these limits, and the only result of this variation in the analysis of the model is a numerical variation in the calculation of the parasitic spreading resistance. The magnitude of the spreading resistance for the case of the flat contact has been calculated by Jeans (13), assuming the conductivity of the metal is infinite:

$$r_s = \frac{\rho}{4r_j} \tag{3-42}$$

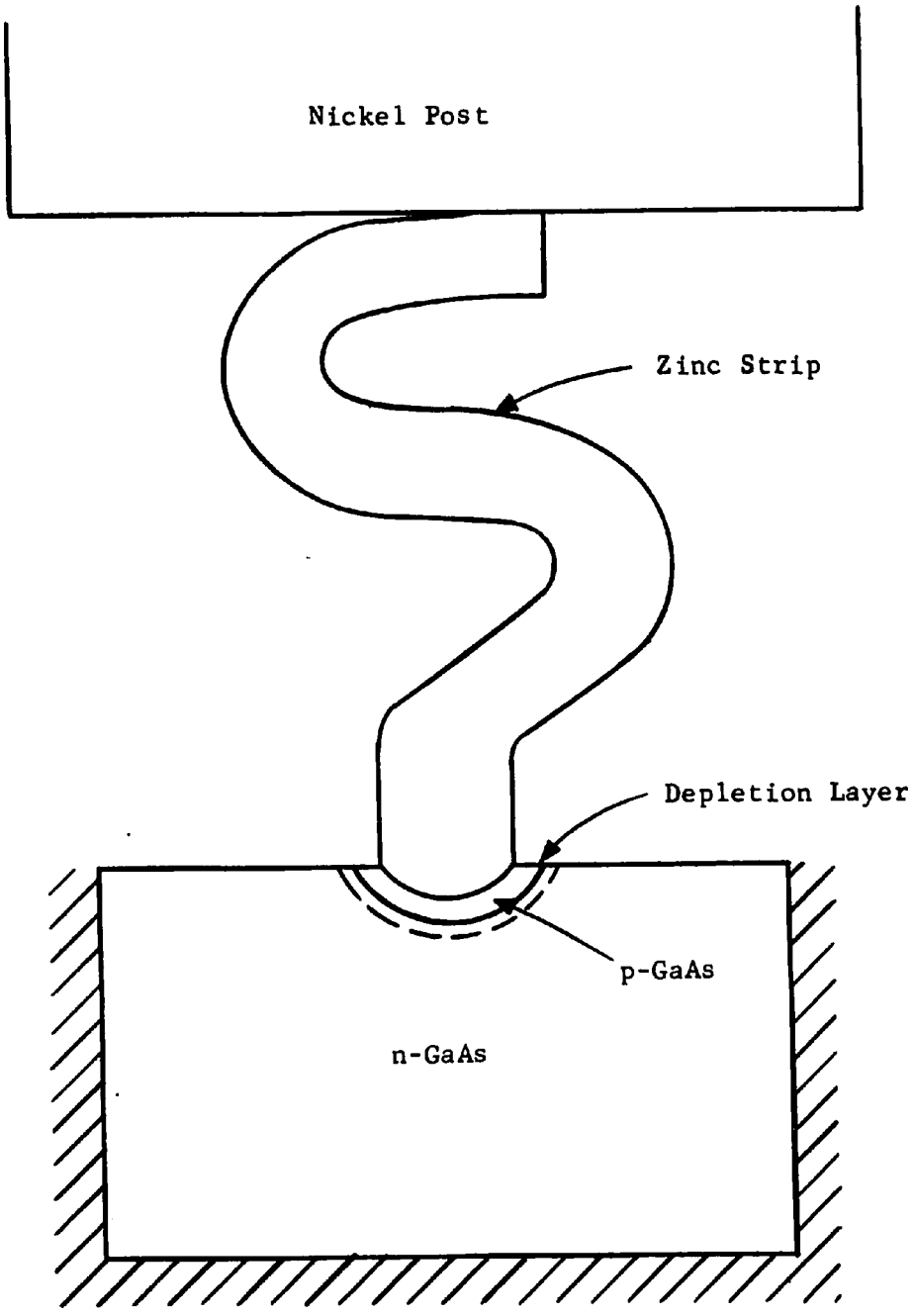

Figure 18 Model of Point Contact Tunnel Diode

where ρ is the bulk resistivity of the semiconductor material

r_j is the radius of the flat circular junction.

The spreading resistance for the hemispherical junction can be approximated as twice the resistance of a spherical junction, which has been calculated by Smythe (30).

$$r_s = \frac{\rho}{2\pi r_j} \tag{3-43}$$

Now as discussed previously, once the semiconducting material is fixed with a certain doping, the product of the negative resistance and the junction capacitance is constant, and the voltage between the peak and valley currents is constant, so that it is convenient to express the resistive cutoff frequency of the tunnel diode in terms of the peak current of the diode. This can be done if the second term of (2-7) is neglected for the parasitic resistance. This term contributes less than ten percent of the total resistance for the diodes used even at 50 Gc/s. Further reduction of this term could be accomplished by reducing the size of the semiconductor chip. The junction radius is proportional to the square root of the peak current. Therefore, the resistance r_s is inversely proportional to the square root of the peak current.

$$r_s = \frac{\alpha}{I_p^{1/2}} \tag{3-44}$$

As an approximation to the maximum negative resistance of the n-type GaAs, the following formula, which fits the experimental curves, is used.

$$R_- = \frac{\Delta V}{2\Delta I} \tag{3-45}$$

Further, the differential current ΔI, which is equal to the peak current minus the valley current, is approximately proportional to the peak

current, since the ratio of the peak current to the valley current is reasonably constant for a given material. Therefore,

$$\Delta I = \gamma I_p \tag{3-46}$$

where

$$\gamma = 1 - \frac{I_v}{I_p} \approx 1 - K .$$

Using this expression, the equation for the cutoff frequency can be written as

$$f_c = \frac{1}{2\pi R_- C}\left(\frac{\Delta V}{2\alpha \gamma I_p^{1/2}} - 1\right)^{1/2} \tag{3-47}$$

or letting

$$K_1 = \frac{1}{2\pi R_- C} \qquad \text{and} \qquad K_2 = \frac{\Delta V}{2\alpha \gamma}$$

then

$$f_c = K_1\left(\frac{K_2}{I_p^{1/2}} - 1\right)^{1/2} . \tag{3-48}$$

Using the approximation used previously,

$$f_c = \frac{K_3}{I_p^{1/4}} \tag{3-49}$$

or

$$I_p = \frac{K_3}{f_c^4} \tag{3-50}$$

and

$$\Delta I = \frac{\gamma K_4}{f_c^4} . \tag{3-51}$$

Now recalling (3-36) and (3-39), the output or load power can be expressed as

$$P_e = \frac{K_5}{f_c^4}\left(1 - \frac{2f^2}{f_c^2}\right) . \tag{3-52}$$

It is possible to determine the maximum power available at a particular frequency if the experimental data are available which gives the resistive cutoff frequency of the tunnel diodes. Thus, in (3-52) considering the frequency of operation as fixed, regarding f_c as a parameter and differentiating (3-52) with respect to f_c yields

$$\frac{dP_e}{df_c} = 0 = \frac{K_4(-4)}{f_c^5}\left(1 - \frac{2f^2}{f_c^2}\right) + \frac{K_4}{f_c^4}(2)\frac{2f^2}{f_c^3} \quad .$$

This requires

$$f_c = 3^{1/2} f \tag{3-53}$$

Substituting this into (3-52) gives

$$P_e = \frac{1}{3}\frac{3}{16}\Delta V \Delta I \quad . \tag{3-54}$$

Thus, the maximum power available for delivery to a load may be written as a function of frequency.

$$P_e = \frac{K_6}{f^4} \tag{3-55}$$

Therefore, the output power available is inversely proportional to the fourth power of frequency, which means that the power is reduced by 40 dB for a decade increase in frequency. This is a severe reduction in power, which is best illustrated by a numerical example. The maximum output power at 50 Gc/s from the experimental results and theory is about 670 μW for n-type GaAs. Using (3-55) it would be expected that the output power at 100 Gc/s would be approximately 28 μW and less than 9 μW at 150 Gc/s.

Equation (3-29), which gives the value of equivalent conductance, is important for circuit considerations. Writing (3-29) in terms of resistance gives

$$R' = 2R_- \quad . \tag{3-56}$$

This requires the equivalent load resistance to be only twice the maximum negative resistance of the diode. It is necessary for R_- to be small to obtain appreciable output power, and this requires low impedance circuits. The actual value of load resistance necessary for the series circuit used in these experiments can be found by substituting (3-24) into (3-56) which gives

$$R = \frac{L}{2R_-C} \tag{3-57}$$

or

$$R = \frac{L\omega d}{2} \quad . \tag{3-58}$$

Recalling that the frequency of oscillation is

$$\omega_o = \frac{1}{(LC)^{1/2}} \quad , \tag{3-59}$$

and replacing L in (3-58) gives

$$R = \frac{\omega_d^2}{2\omega_o^2} R_- \quad . \tag{3-60}$$

This requires the actual resistance to be smaller than the negative resistance of the diode for the millimeter frequencies since $\omega_o > \omega_d$. If a diode with a differential current ΔI equal to two milliamperes, and operating at 50 Gc/s is considered, R should be approximately 25 ohms.

CHAPTER IV

EXPERIMENTAL PROCEDURE

Diode Fabrication

The n-type GaAs tunnel diodes used were made from highly polycrystalline material which originated from two sources. One source was C. A. Burrus (4) of the Bell Telephone Laboratories. Burrus prepared the semiconducting material by melting a few grams of GaAs with an excess of selenium, or selenium and tellurium in an evacuated quartz ampule. The second source of semiconducting material was the Monsanto Chemical Company in St. Louis, Missouri. The semiconductor was prepared at Monsanto by pulling a small ingot from a large melt containing 5 weight per cent selenium. These materials were so polycrystalline that reliable measurements of carrier concentration were not possible. However, n-type GaAs epitaxial layers containing more than 1.6×10^{19} donors per cubic centimeter (as measured by Monsanto) made tunnel diodes which did not exhibit negative resistance at 50 Gc/s (39), and it is estimated that the n-type GaAs useful for millimeter wave frequencies must contain donor concentrations approaching $4\text{-}5 \times 10^{19}$ donors per cubic centimeter, a value above the range normally achieved in a single crystal GaAs (37) sample.

The back contact (ohmic contact) for the diodes used in this investigation was essentially the same as the one used by Sharpless (28). Slices of the doped semiconductor were etched, electroplated with tin, alloyed in vacuum, and plated with nickel. The slices were then diced into squares approximately 0.010 inches across, and the dicings were soldered to the end of a nickel post 0.030 inches in diameter and placed in various waveguide circuits through a suitable by-pass capacitor to allow for bias application. The semiconductor was approximately flush with the waveguide wall. The contact for the semiconductor junction was made by a pressure contact of a strip of zinc foil. The zinc strips were approximately 0.005 inches thick, 0.002 inches wide, and 0.015 to 0.020 inches long. The narrow width was obtained by placing a piece of foil between two microscope slides and cutting a strip with a razor blade. Uniform strips could be obtained fairly readily in this manner. The zinc strip was soldered to the end of a 0.030 inch diameter nickel post, and needle-point tweezers were used to bend the zinc strip into the shape shown in Figure 19-a. After the zinc strip was bent a diagonal cut was made with a pair of cuticle scissors to obtain the sharp point shown in Figure 19-b. This operation was done under a microscope with a magnification of about 30. Surprisingly enough, this operation was fairly easy and could be done rapidly after a few days practice. The next operation was to insert the nickel post with the zinc strip through a hole in the broad face of the waveguide. The hole in the waveguide was only slightly larger in diameter than the nickel post, and ideally, a tight press fit could be obtained. With a thin waveguide wall, so that the length of contact between the nickel post and waveguide wall

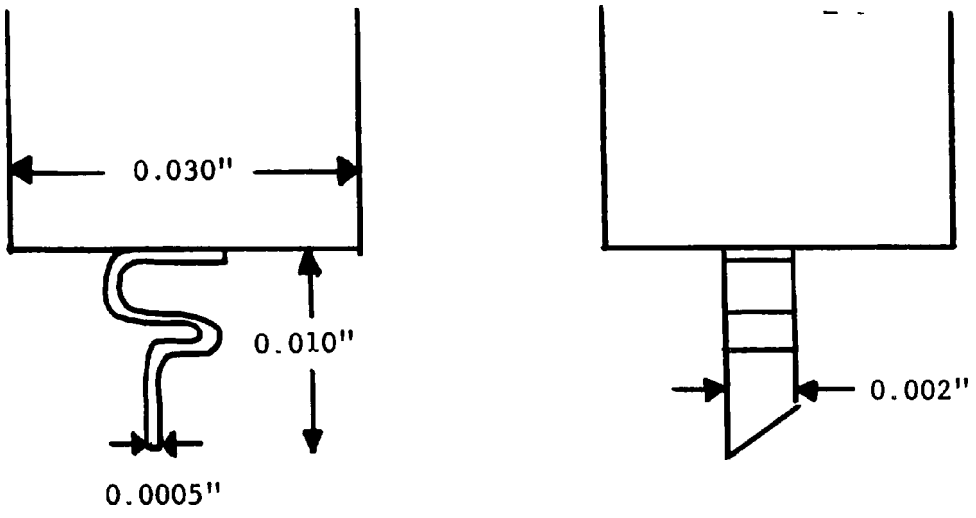

Figure 19 Shape of Zinc Strip

was short, it became necessary to knurl the nickel post. The knurling could be accomplished by rolling the post over a flat surface beneath a fine file. Considerable care had to be taken to insure that the fit was loose enough for the post to slide in the waveguide hole. This was a problem with the wafer waveguide structure because a tight post would deform the waveguide, and make it impossible to obtain the proper contact to the semiconductor. The post was pushed through the waveguide hole until the zinc strip was visible inside the waveguide and almost touching the semiconductor. Next, a 60 c/s sinusoidal voltage was applied between the semiconductor and the post with the zinc strip as shown in Figure 20. The 60 c/s voltage was obtained from the circuit shown in Figure 21. The circuit shown in Figure 21 allows the volt-ampere characteristic of the diode to be displayed on an oscilloscope by taking a voltage equal to the diode voltage and applying it to the horizontal amplifier of the oscilloscope. A voltage proportional to the

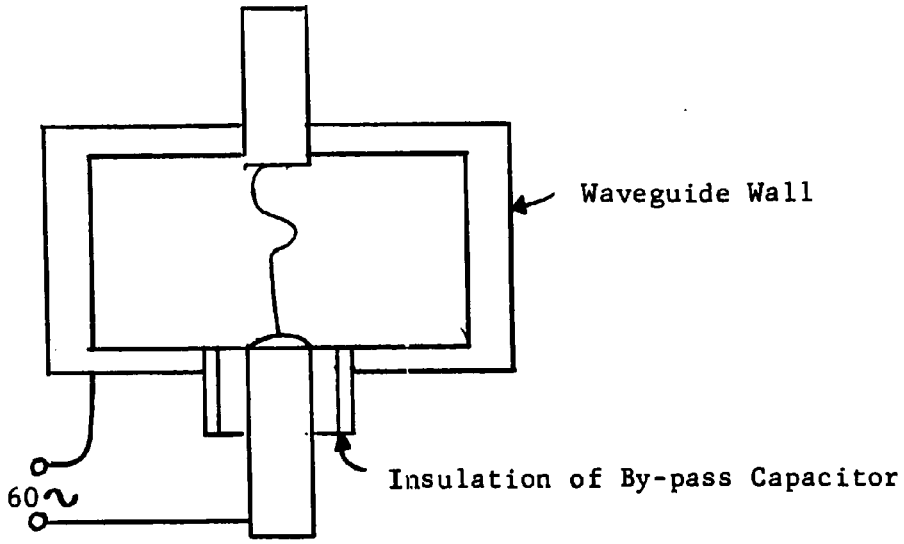

Figure 20 Bias Application for Display

diode current was applied to the vertical amplifier of the oscilloscope. The post with the zinc strip was adjusted to contact the semiconductor, while the volt-ampere characteristic was observed on the oscilloscope. This adjustment was probably the most important part of the diode fabrication. It was essential to have the mechanical pressure at the contact between the zinc and the semiconductor correct. The pressure must be high enough to insure a stable contact free of erratic electrical behavior, but it still should be as light as possible to prevent an ohmic contact. The proper pressure could be obtained by observing the oscilloscope. Figure 22 shows a diode characteristic with the contact pressure too low. Figure 23 shows a diode characteristic with too much pressure at the contact. This contact is practically an ohmic contact, and it is not possible to make good tunnel diodes from such a contact.

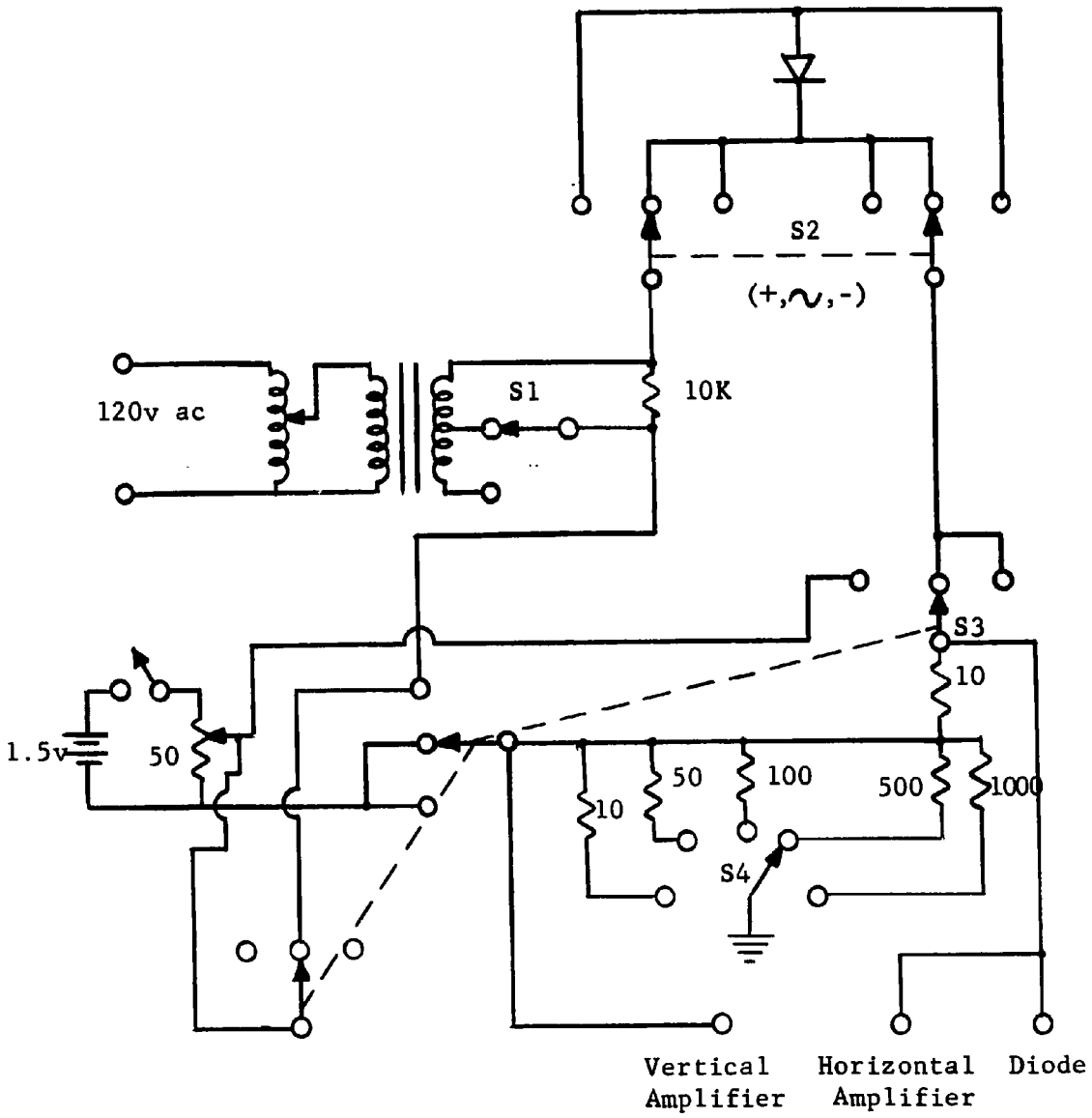

Figure 21 Circuit for Diode Display

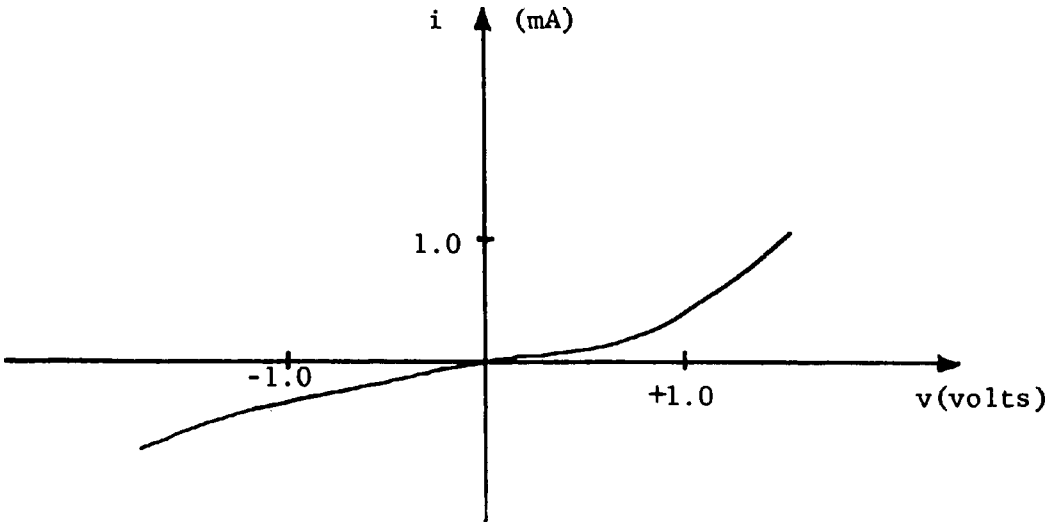

Figure 22 Low Contact Pressure

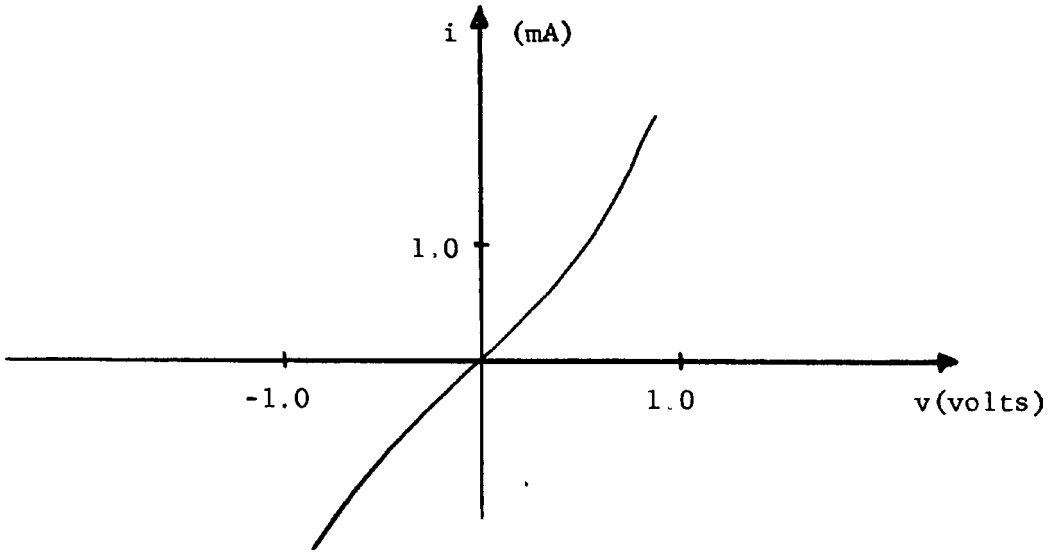

Figure 23 High Contact Pressure

Figure 24 shows the volt-ampere characteristic for the metal-semiconductor junction when the pressure is correct. This characteristic has a very sharp break in the forward bias region and can be used as a

variable capacitance or variable resistance diode. Once the contact pressure was correct, a voltage pulse was applied to the diode in the reverse direction. This voltage pulse was obtained from a simple resistance capacitance circuit shown in Figure 25 for low peak current tunnel diodes. The variable capacitance is connected to the source to charge to a voltage of approximately 5 volts. The pulse is obtained by switching

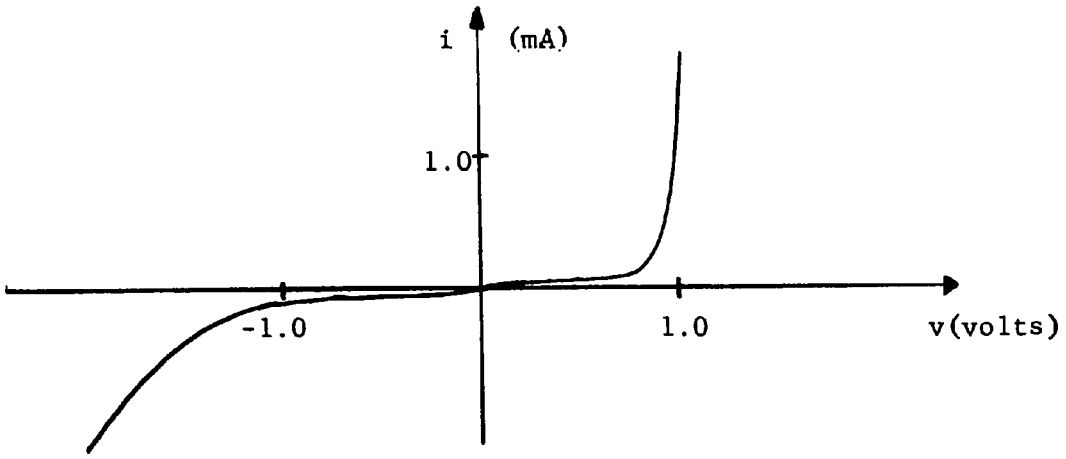

Figure 24 Correct Contact Pressure

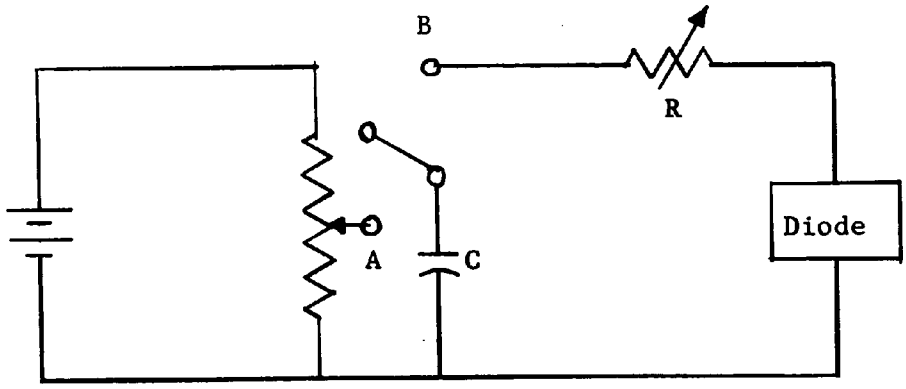

Figure 25 Pulse Circuit for Low Peak Current Diodes

the charged capacitor to the point marked B in Figure 25. The best diodes were obtained when the capacitance was about 0.01 μF, and the resistance was approximately 50 ohms. The peak currents of the tunnel diodes tended to vary directly with the magnitude of the voltage, and inversely with the resistance. It was possible to adjust the peak current from a few hundred microamperes to about 7 milliamperes. Diodes with peak currents higher than 7 milliamperes degraded almost instantaneously, and it was impossible to use them. Useful diodes for X-band frequencies could be made with peak currents up to approximately 30 milliamperes by a different pulse technique. This pulse was obtained from the one shot multivibrator shown in Figure 26. The X-band frequency

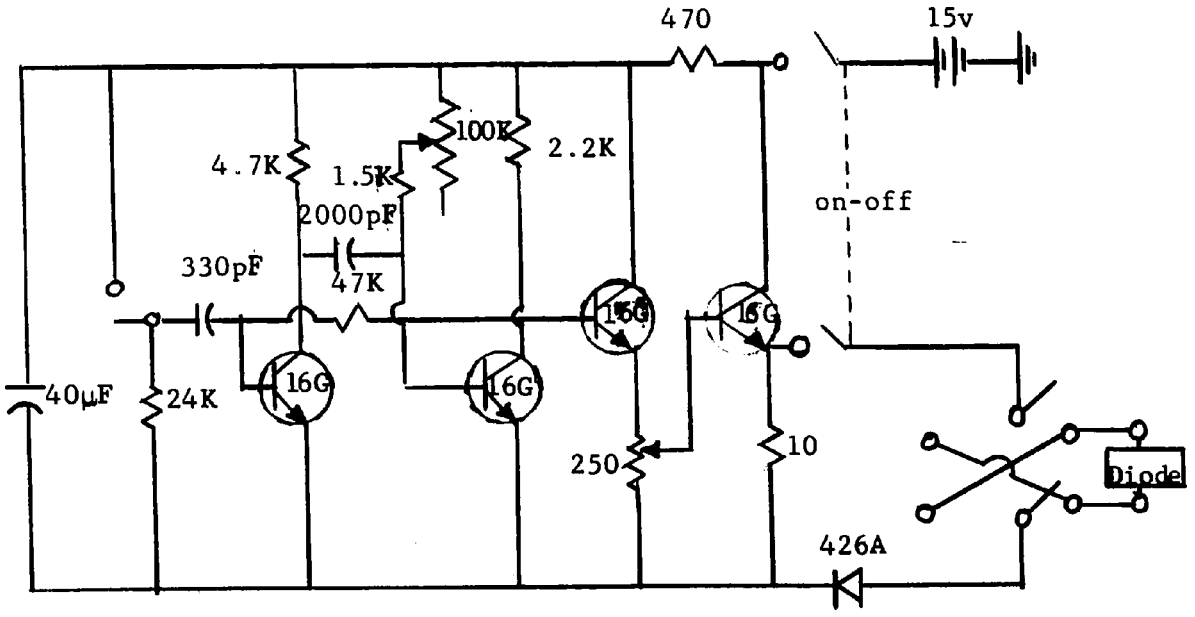

Figure 26 Pulse Circuit for High Peak Current Diodes

tunnel diodes could be made by repeated pulsing which allowed a reasonably careful adjustment of the peak current to be attained. The useful diodes for the millimeter frequencies were formed with only one pulse. After making several hundred low peak current diodes, no oscillations were obtained when the diode had more than one forming pulse. This was a problem when a specific peak current was desired for a high frequency diode. It was often necessary to make several tries to obtain a specific peak current. The fabrication of these diodes was very sensitive to the initial pressure of the contact, the initial cleanliness of the semiconductor surface, and the pulse forming conditions.

Waveguide Circuits

The waveguide circuits were somewhat varied, but were similar in the following respect; the diode was located in a section of rectangular waveguide with the height reduced. The reduced height was about one-eighth the normal height of approximately one-half the width, except the X-band wafer circuit. The reduced height waveguide was connected to a well matched tapered waveguide which tapered to a standard height at one end.

The various waveguide circuits used are shown in the figures below. The first and simplest circuit is shown in Figure 27. The width of the guide is the standard X-band width of 0.900 inches and the height is 0.050 inches. The impedance of this guide was about 50 ohms at midband and Figure 28 shows the impedance as a function of frequency. Concentric holes were drilled in the broad faces of the waveguide. One hole was approximately 0.031 inches in diameter to allow a tight press fit with the 0.030 inch diameter nickel post with the zinc point contact.

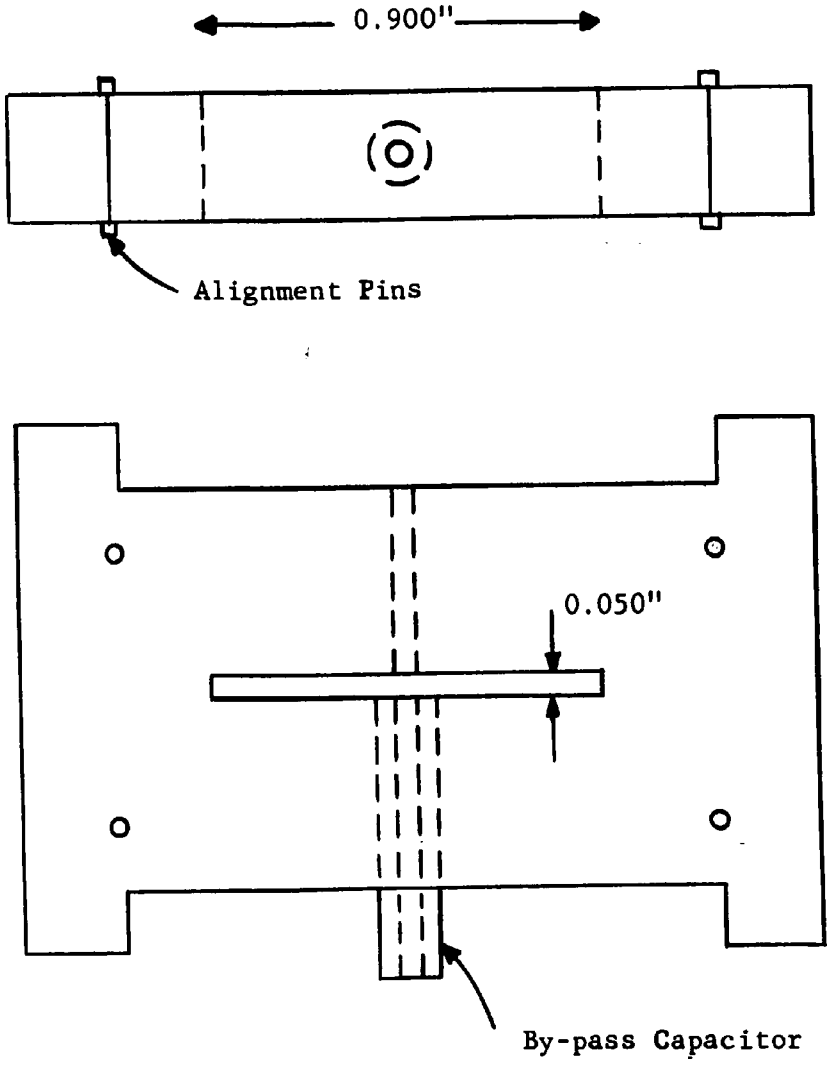

Figure 27 X-Band Waveguide Diode Holder

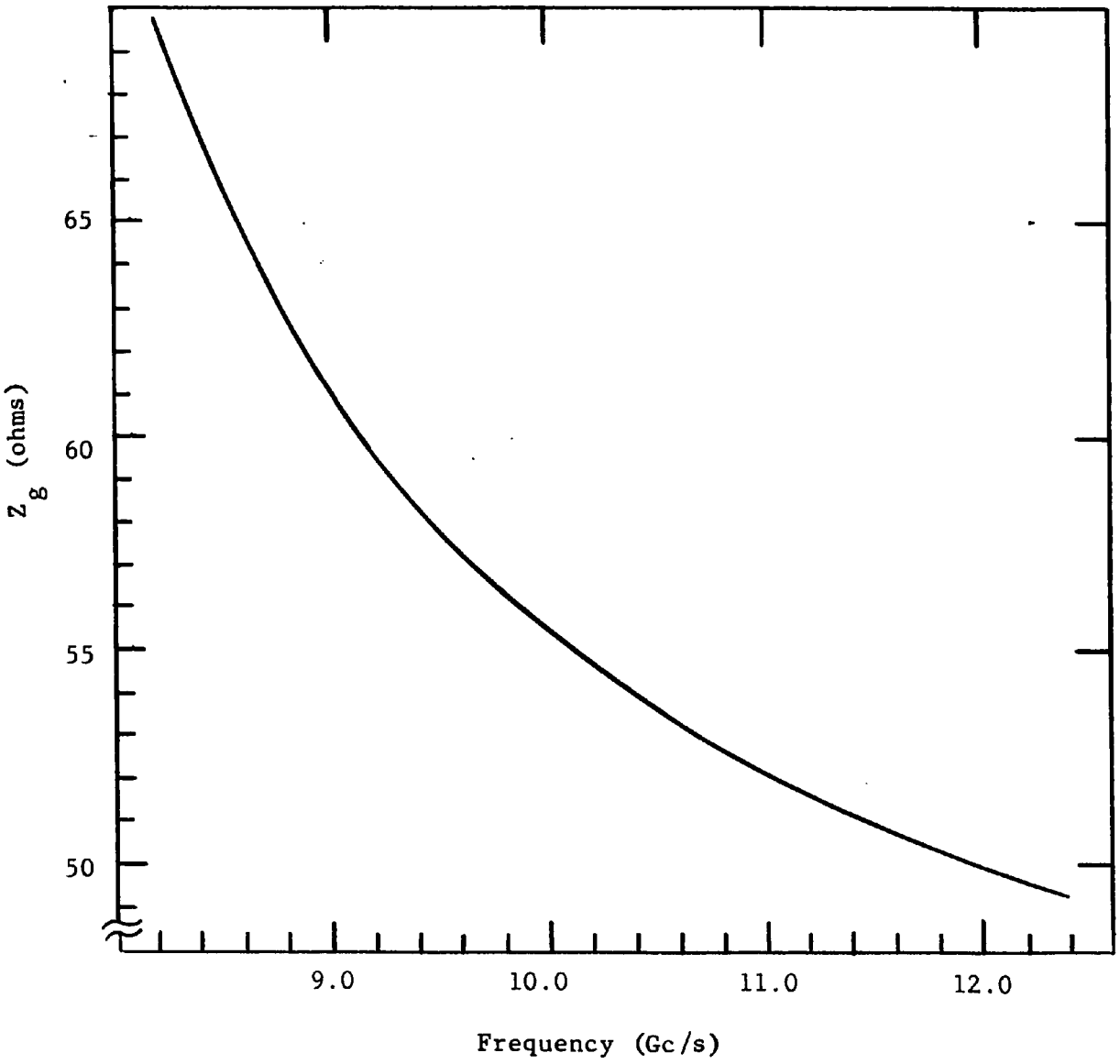

Figure 28 Impedance of 0.050 Inch X-Band Guide

The opposite hole was considerably larger to allow some type of by-pass capacitor to insulate the nickel post containing the semiconductor chip from the waveguide. This was necessary so that dc bias could be applied to bias the diode in the negative resistance region. Several insulating materials were tried for the capacitor, including Rexolite, mylar, epoxy and aluminum oxide. The most satisfactory capacitors for the X-band circuits were the anodized aluminum capacitors developed by Braun and Trambarulo (1). These capacitors are constructed like a coaxial transmission line and in fact, are useful as low impedance (1 ohm) coaxial transmission lines. The capacitors were approximately 0.12 inches in diameter, and the center conductor was about 0.10 inches in diameter. A 0.031 inch diameter hole was drilled in the center conductor, and the nickel post with the semiconductor chip could be press fitted into the capacitor hole as shown in Figure 29, after the capacitor had been pressed into the hole in the waveguide wall. Epoxy was satisfactory at the millimeter frequency, but the removal of the semiconductor for chemical etching was difficult. The 0.050 inch waveguide was connected on either side to a raised cosine taper (2) from the 0.050 inch high waveguide to the standard 0.400 inch waveguide. Although oscillation was

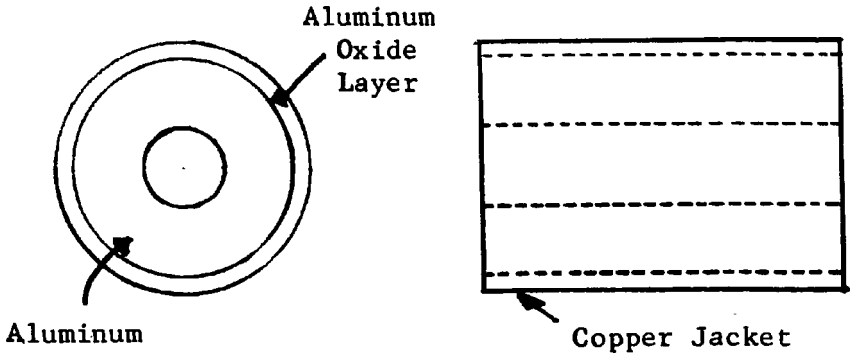

Figure 29 By-pass Capacitor

possible in this circuit, it was primarily useful in the transmission resonance measurements to characterize the diodes and to determine the equivalent circuits. The most useful X-band oscillator circuit is shown in Figure 30. The thin section of guide was 0.010 inches high and the width was one and one-half times the width of the connecting waveguide. The impedance of this guide was one-fifth the impedance of the 0.050 inch high waveguide. The holes through the waveguide were one-third the width of the waveguide from the waveguide wall. When the thin section of waveguide was pushed completely into the holder, the position of the diode was the center of the connecting waveguide. As the thin section of waveguide was pulled out of the holder, the position of the diode with respect to the connecting waveguide could be varied continuously from the center of the waveguide to the waveguide wall. This allowed a very important adjustment of the impedance seen by the diode. This tuning adjustment made it possible to present the proper impedance to the diodes to obtain the maximum output power. The connecting waveguide in the front section of the holder was a linear taper from the 0.010 inch height to a height of 0.050 inches to connect to the raised cosine taper to standard waveguide. The connecting waveguide in the back section of the holder was a straight section 0.010 inches high. A short-circuiting piston was placed in this waveguide to provide impedance and frequency tuning. This piston was a contacting type. The piston was constructed by bending strips of contacting metal 0.001 inch thick into loops and soldering these loops between the sheets of copper, as shown in Figure 31. These pistons worked satisfactorily, but they were fragile, and fairly difficult to construct. A crude piston was

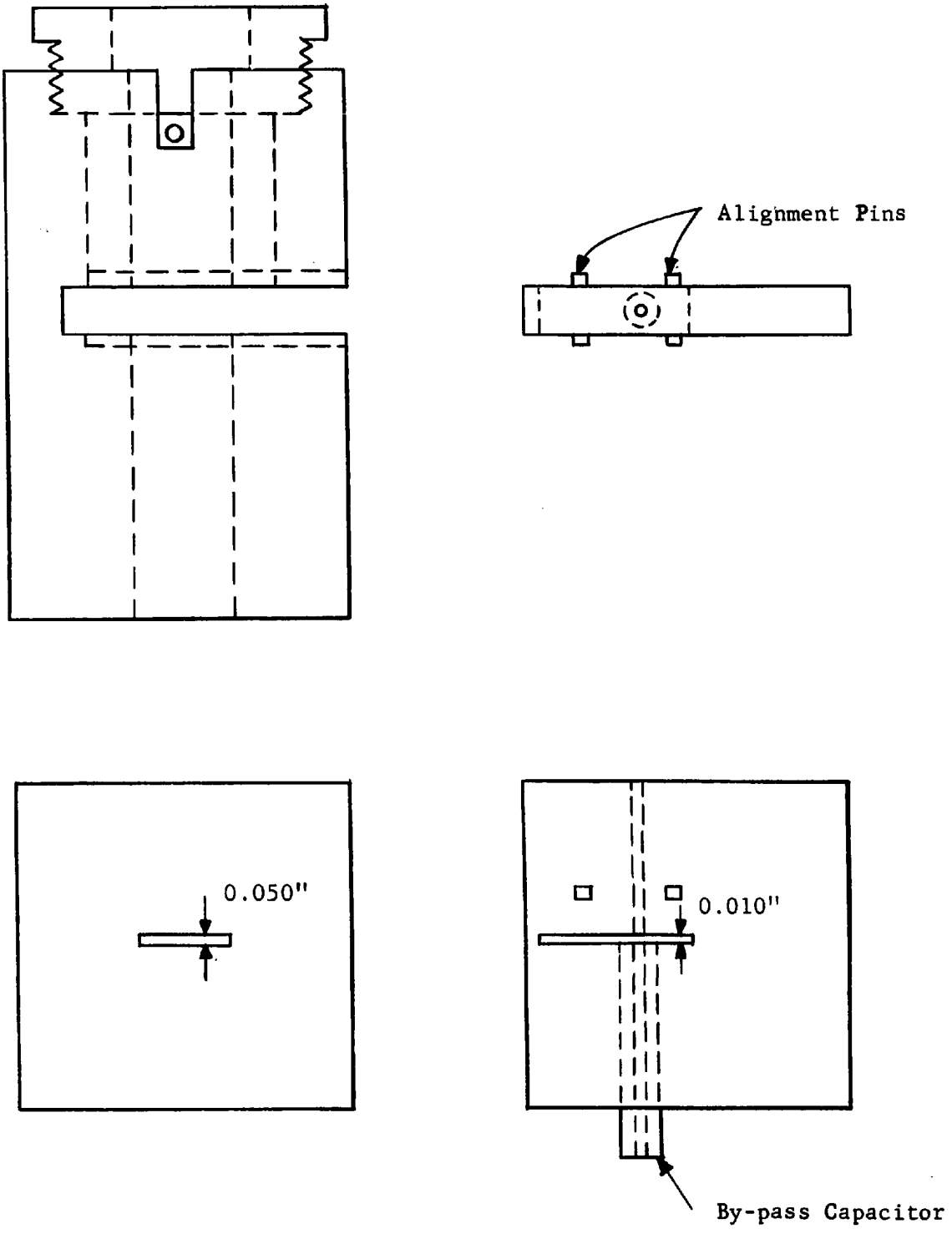

Figure 30 X-Band Wafer Circuit

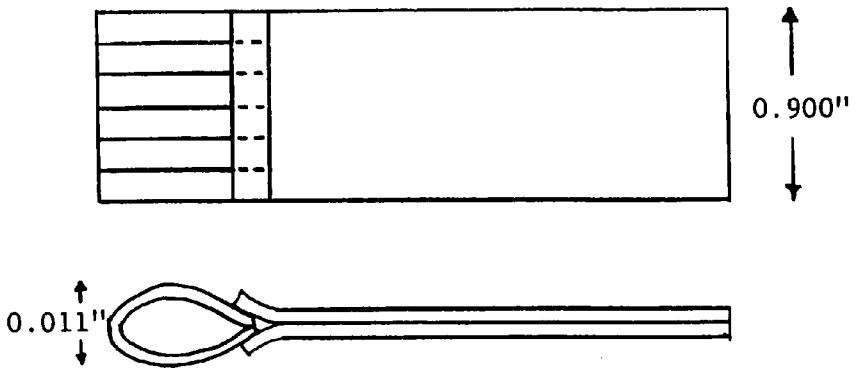

Figure 31 X-Band Piston

made by bending a strip of beryllium copper (0.002 inches thick and 0.900 inches wide) double, as shown in Figure 32. The straight millimeter frequency waveguide diode holder is shown in Figure 33. The width

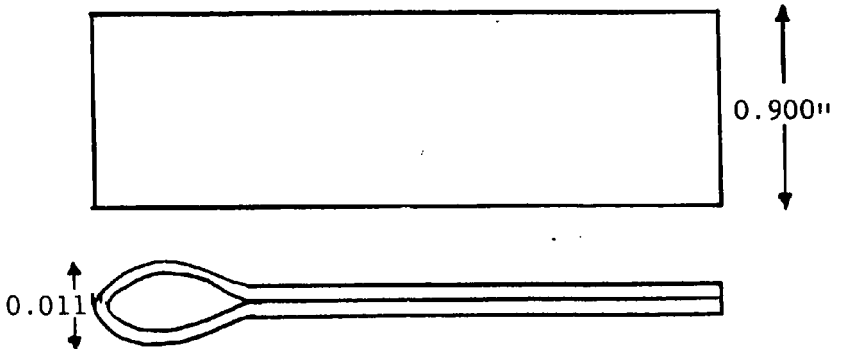

Figure 32 Simple X-Band Piston

of the waveguide is 0.148 inches, which is the standard RG98/U waveguide width. This waveguide is designed for a single mode operation between 50 Gc/s and 75 Gc/s with a cutoff frequency just below 40 Gc/s. The height of the waveguide is 0.010 inches. The impedance of this guide

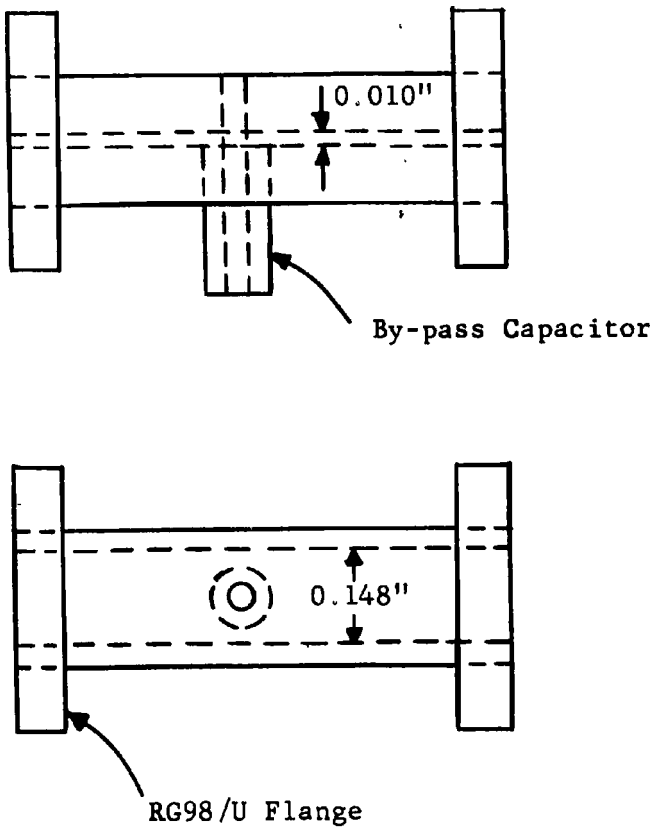

Figure 33 Millimeter Waveguide Diode Holder

is about 65 ohms at the midband frequency, and a plot of the waveguide impedance versus frequency is shown in Figure 34. This straight waveguide circuit was used in the transmission resonance measurements between 50 Gc/s and 70 Gc/s. These straight waveguide sections were connected to tapers to obtain the normal waveguide height of 0.074 inches. Figure 35 shows some ridge waveguide components built for millimeter frequencies. The ridge waveguide section diode holder had a 0.010 inch spacing, and it provided a waveguide impedance of only 40 ohms. The important difference between the ridge waveguide and the rectangular waveguide was the reduction of the cutoff frequency. This ridge waveguide had a cutoff frequency below 20 Gc/s, and diode oscillation below the waveguide frequency was not possible. The waveguide circuit shown in Figure 36 was the most useful circuit for tunnel diode oscillators at the millimeter frequencies. It was similar to the X-band circuits, which allowed the diode to be horizontally positioned to obtain the maximum power output. This circuit was a modification of a design used by Sharpless (27), for resistive point contact diodes. Most of the waveguide wafers had a 0.010 inch high waveguide, and a waveguide width one and one-half times the standard RG98/U width of 0.148 inches. A few wafers had 0.008 inch high waveguide, but the fabrication of good diodes with the zinc strip less than 0.010 inches after bending was difficult. It was also very difficult to machine the 0.008 inch waveguide, and the alignment of the wafer to the connecting waveguide was not too good.

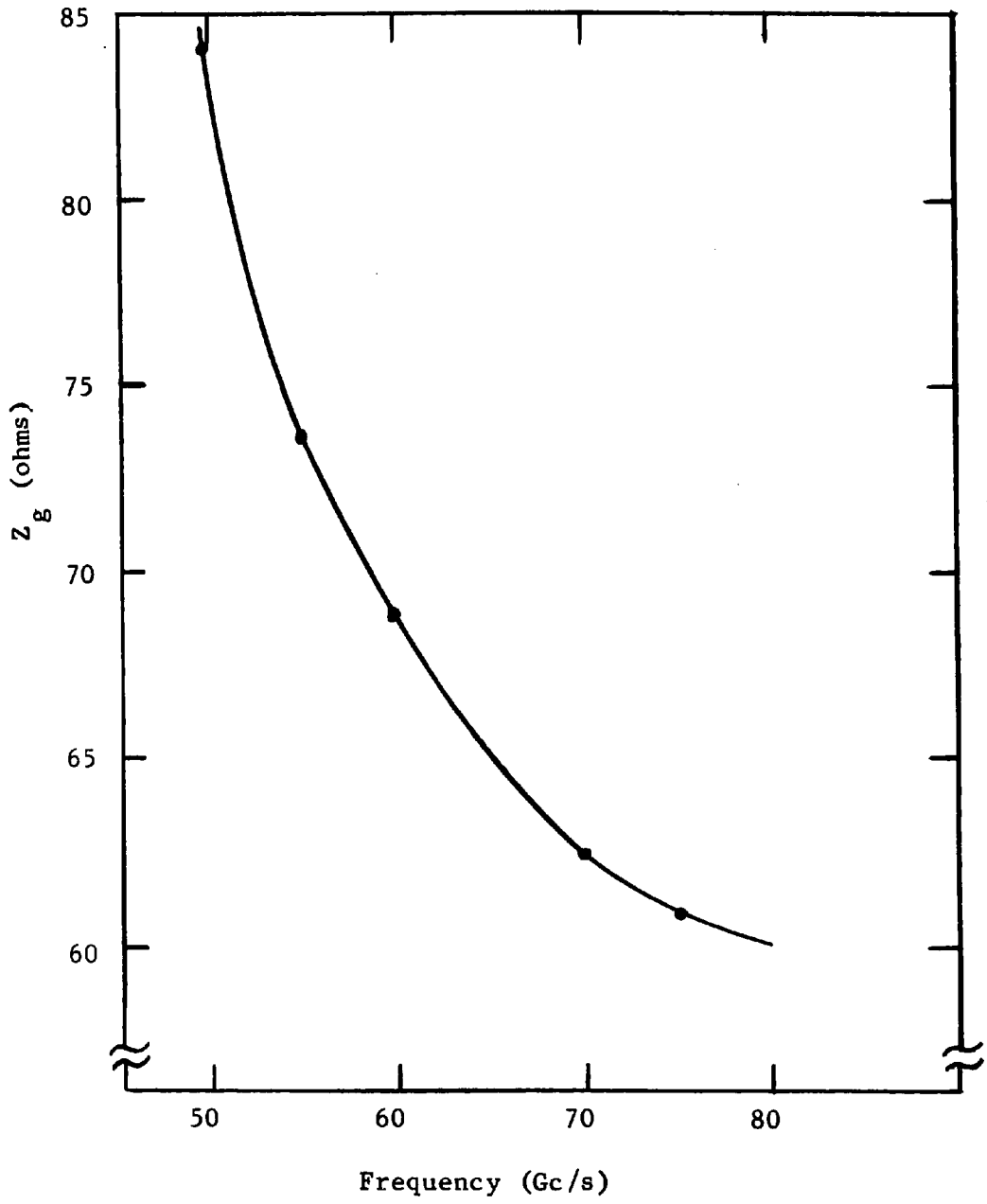

Figure 34 Impedance of 0.010 Inch Millimeter Waveguide

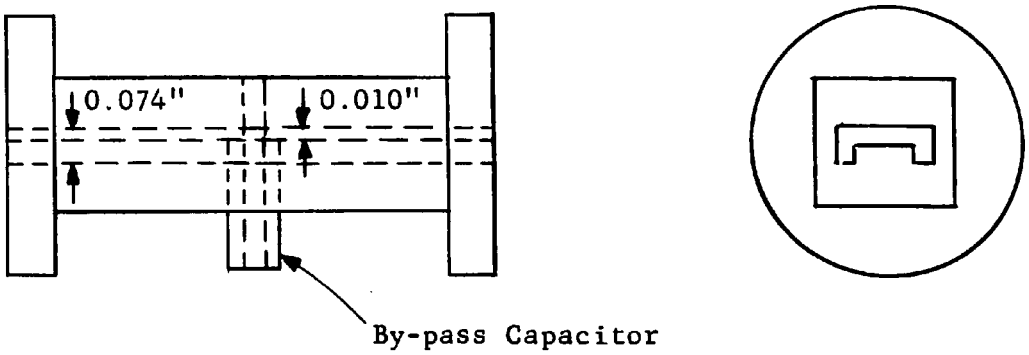

(a) Diode Holder

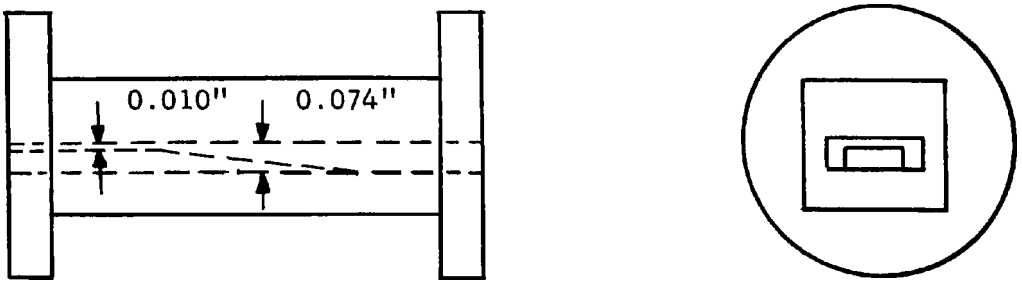

(b) Taper

Figure 35 Ridge Waveguide Components

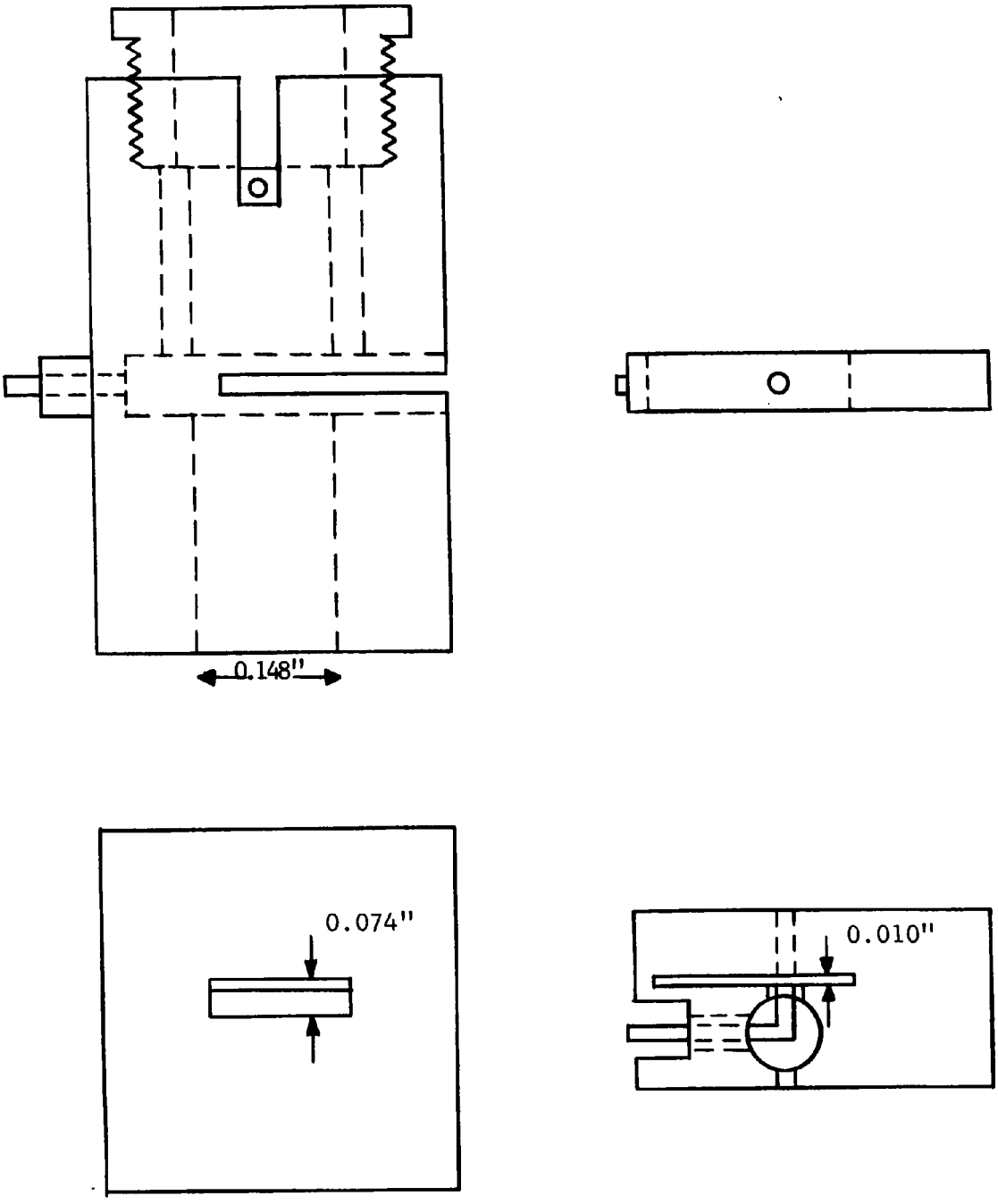

Figure 36 Millimeter Wafer Circuit

Electrical Measurements

The electrical measurements of the diodes were essentially divided into two categories. One set of measurements consisted of measuring the equivalent circuits of the diodes. The second set of measurements consisted of measuring the absolute power output, and the frequency of oscillation of the tunnel diode oscillators. The measurements at the millimeter frequencies were essentially the same as the measurements at X-band, and only the X-band measurements will be discussed in detail. The measurements of the equivalent circuit parameters of the diodes were made by the transmission resonance technique (3). The block diagram of the system for this measurement is shown in Figure 37. The X-band oscillator was swept with a 60 c/s voltage from 8.5 Gc/s to 12.4 Gc/s. The output from a baseband detector from the RF path which included the diode was compared to the output of a baseband detector from a reference path. The two detector outputs were balanced with the diode removed. The tunnel diodes were biased at the peak or valley current points of the volt-ampere characteristic. The transmission loss versus frequency was measured by adjusting a precision RF attenuator in either the unknown or the reference path. It was necessary to measure the transmission loss at three frequencies to determine the diode spreading resistance, the diode junction capacitance, and the inductance of the zinc strip in the waveguide. While it was possible to use any three frequencies, the best experimental results were obtained when the resonant frequency of the inductance and junction capacitance was in the frequency band of the oscillator. The length of the zinc strip could be valued from about 0.010 to 0.050 inches. This varied the inductance by

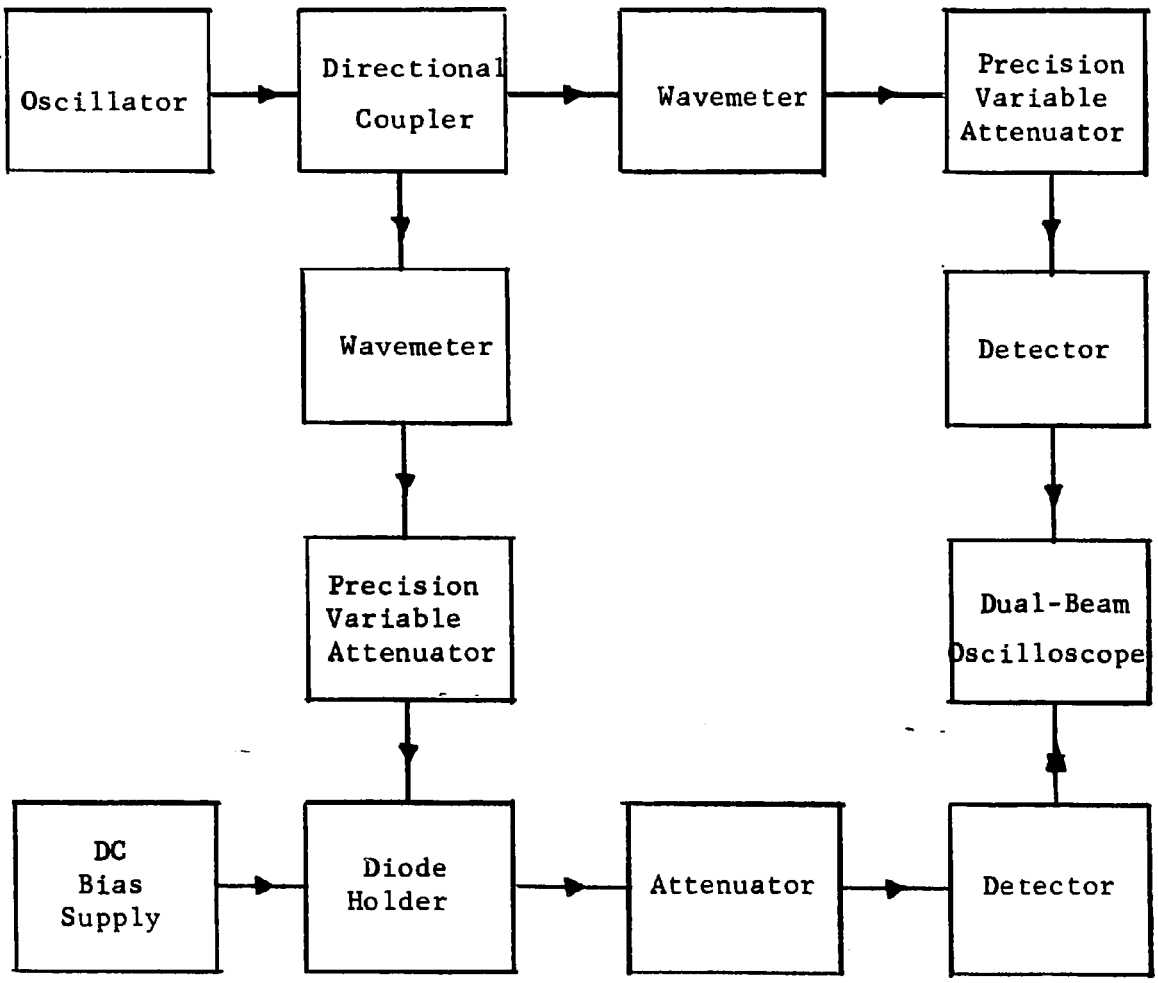

Figure 37 X-Band Transmission Resonance System

approximately one order of magnitude from 10^{-10} henries to 10^{-9} henries. This allowed a resonance in the frequency band 8.5 Gc/s to 12.4 Gc/s for capacitance values between 0.17 pF and 3.5 pF, which meant a considerable range of peak currents for the diodes. Two very important requirements had to be met in performing the measurement of the diode parameters. Since the theory is based on a small signal variation about the bias point of the diode, the RF power on the diode had to be as low as the measurement sensitivity allowed. The incident power on the diodes was usually below 1 μW. It was still difficult to keep the diodes biased at the peak current long enough to complete the measurement. It was also important to keep the diodes biased as close as possible to the maximum or minimum current values to satisfy the theoretical assumption of infinite barrier resistance. This condition was much easier to satisfy at the minimum current bias.

The measurement of output power and the frequency of oscillation was accomplished with the simple circuit shown in block diagram form in Figure 38. The diode was biased with a 60 c/s voltage large enough to sweep the diode voltage from zero to the forward injection region through the negative resistance region. While the diode was biased in the negative resistance region RF oscillation was usually obtained. The power output from the oscillation was applied to a detector diode, and the rectified 60 c/s voltage output was applied to a dual beam oscilloscope. This detected power output and the volt-ampere characteristic were displayed simultaneously on the oscilloscope. A typical oscillator diode characteristic and detected RF output power versus diode voltage are shown in Figure 39. This particular diode was oscillating above the

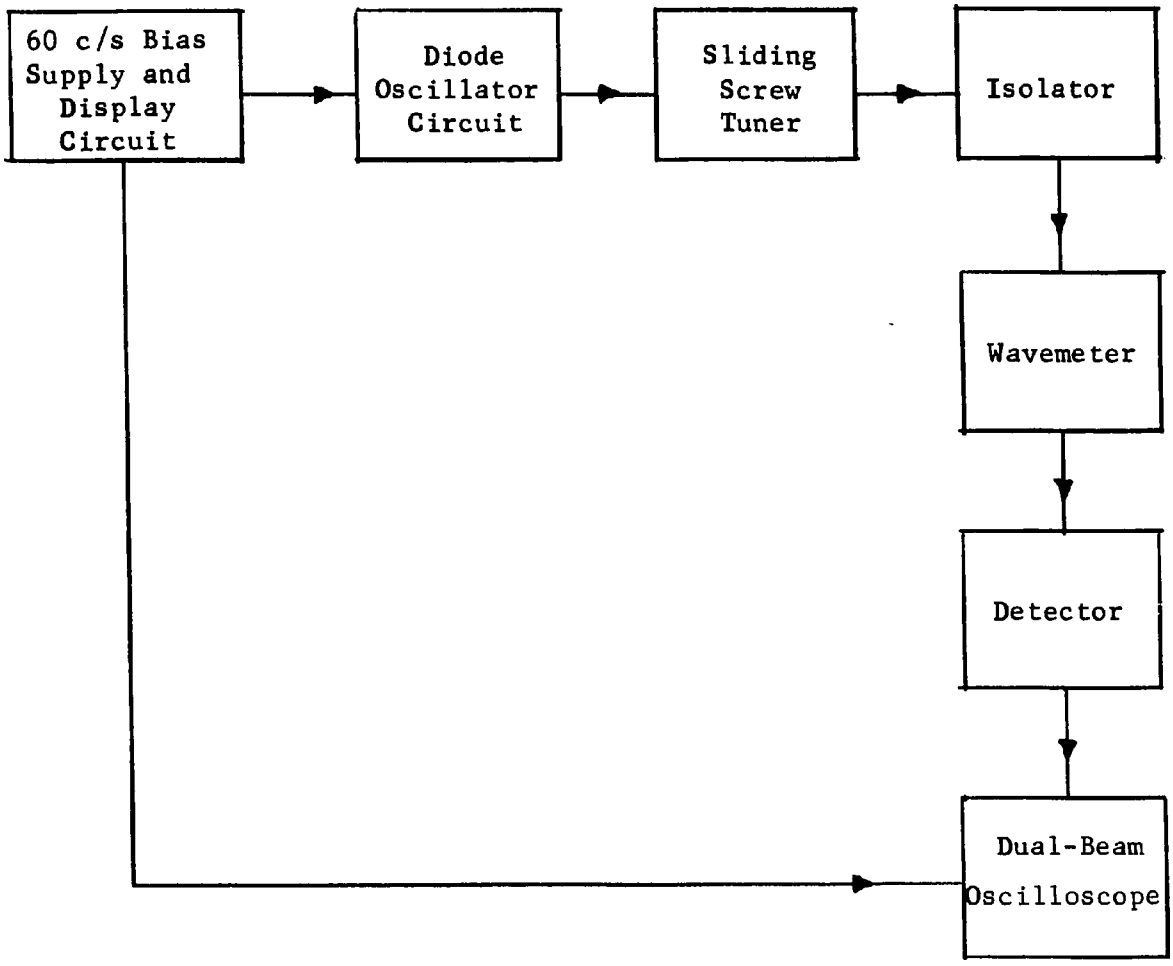

Figure 38 Oscillator System Block Diagram

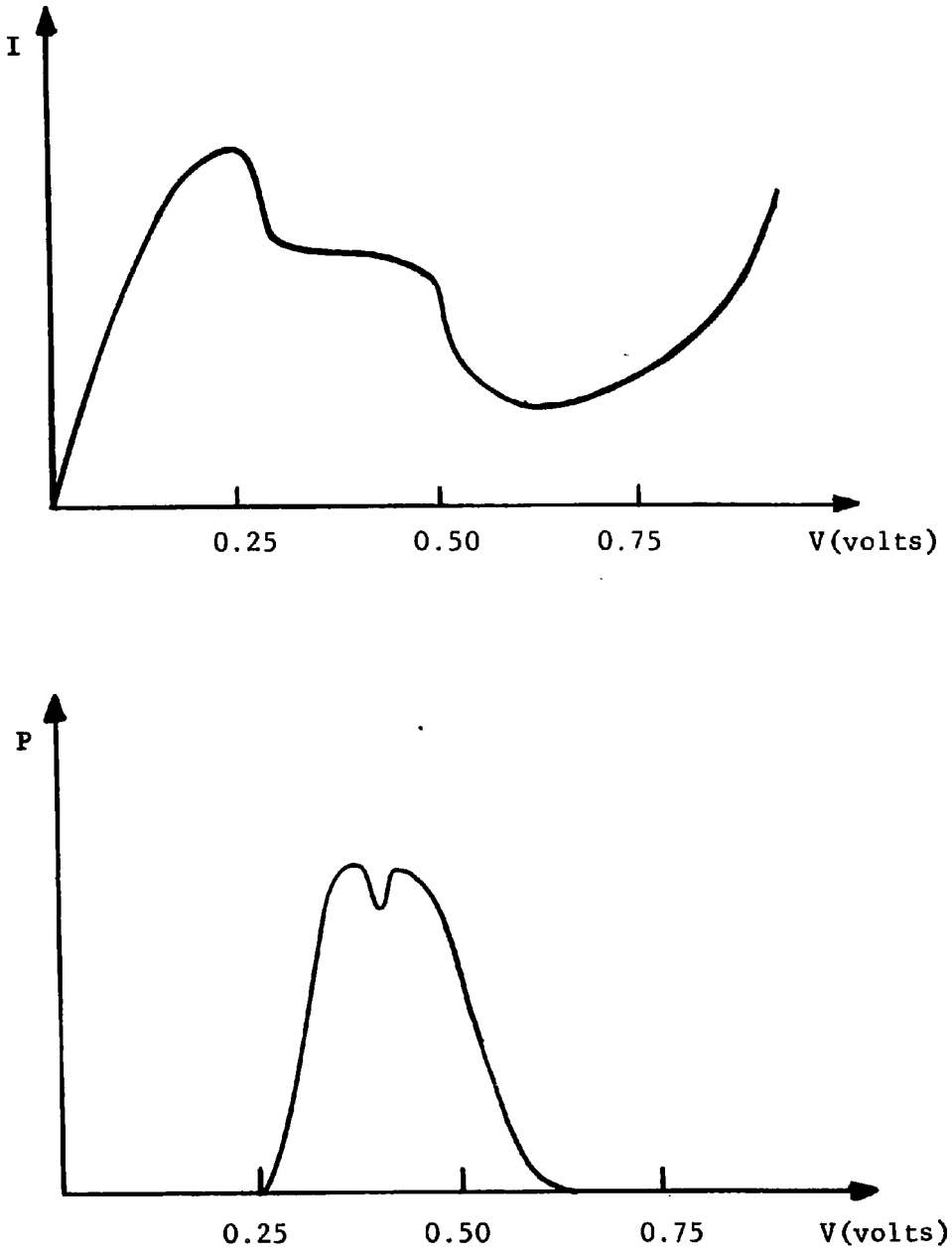

Figure 39 Oscillator Diode Current and Power Output Versus Diode Voltage (Fundamental Oscillation)

waveguide cutoff frequency. The dip in the power output was due to some of the output power dissipated in the RF wavemeter, which was between the oscillating diode and the detector diode. Figure 40 shows a diode which was oscillating below the waveguide cutoff frequency. The power output shown was at the second harmonic of the actual oscillation frequency. This condition was usually undesirable, although some preliminary experiments were performed using this situation as a frequency converter. A signal above the waveguide cutoff frequency was mixed with the oscillation frequency, and the predicted difference frequency was obtained in the bias circuit.

The most troublesome part of the oscillator experiments was the elimination of any oscillation in the bias circuit. The tunnel diodes presented a negative resistance at all frequencies below the cutoff frequency, and it was necessary to provide stabilization outside the waveguide circuit. A sufficiently small resistor was located as close as physically possible to the diode. This was satisfactory if the peak current of the diode was small enough in a particular waveguide circuit. A physical example of a simple stabilizing resistor is shown in Figure 41. The resistance in this case was provided by a pencil lead located in the wafer circuit as shown in Figure 41. This circuit was the one used to obtain the maximum power output at 50 Gc/s.

The frequency of oscillation was obtained by observing a wavemeter pip in the output power displayed on the oscilloscope. These frequency measurements were checked by measuring the guide wavelength in the following manner. The probe of a slide screw tuner was inserted into the guide near the diode oscillator until the output power pattern was changed

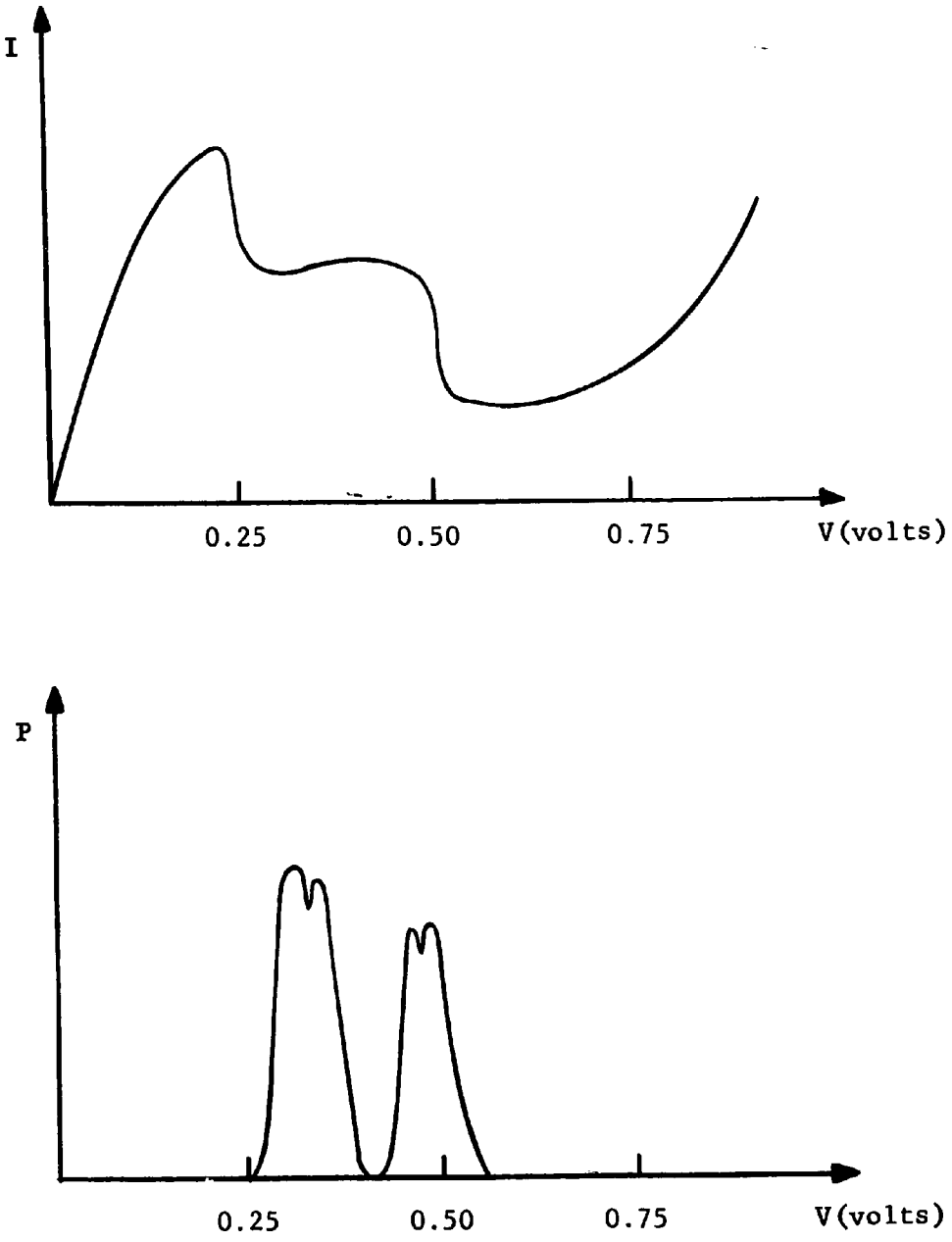

Figure 40 Oscillator Diode Current and Power Output Versus Diode Voltage (Harmonic Output)

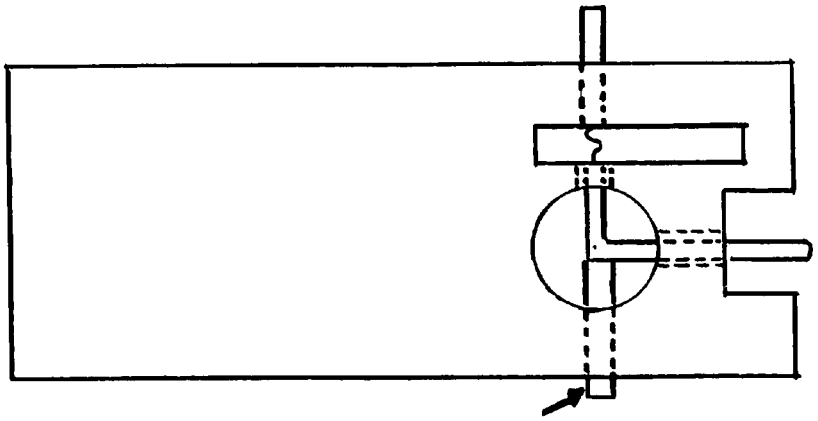

Figure 41 Oscillator Diode Holder with Stabilizing Resistor

on the oscilloscope. As the probe was moved along the guide axis, the power output would vary until the probe had travelled one-half a guide wavelength. This was a necessary verification of the wavemeter reading, because of the wavemeter resonances above the calibrated frequency band.

The most important electrical measurement for the oscillator diodes was the measurement of absolute power. The power measurements were made with a precision rotary vane RF attenuator and a detector diode. The attenuator was calibrated in a double detection set against a calibrated 70 Mc/s attenuator. The detector diode was calibrated against a commercial power meter at X-band, and against a calorimeter built by Sharpless (28) for the 50 Gc/s to 60 Gc/s frequency range. The calibration power level was one milliwatt in both cases. A plot of the output voltage versus RF power input of the X-band detector diode connected

to a high impedance oscilloscope is shown in Figure 42. An isolator was permanently attached in front of the calibrated detector diodes, and periodic checks were made against the standards to insure as much accuracy as possible in the power measurements.

Rather extensive measurements were taken to determine the electrical life of the millimeter frequency diode oscillators. The circuit used is shown in Figure 43. Each diode was biased in the negative resistance region for maximum output power with a dc bias, and allowed to run continuously. The power output was detected with a detector diode connected to a low impedance microammeter. The output power was recorded approximately twice a day. Figure 44 is a plot of the output power versus time of one of the better 50 Gc/s diode oscillators. Several diode oscillators were tested in this manner.

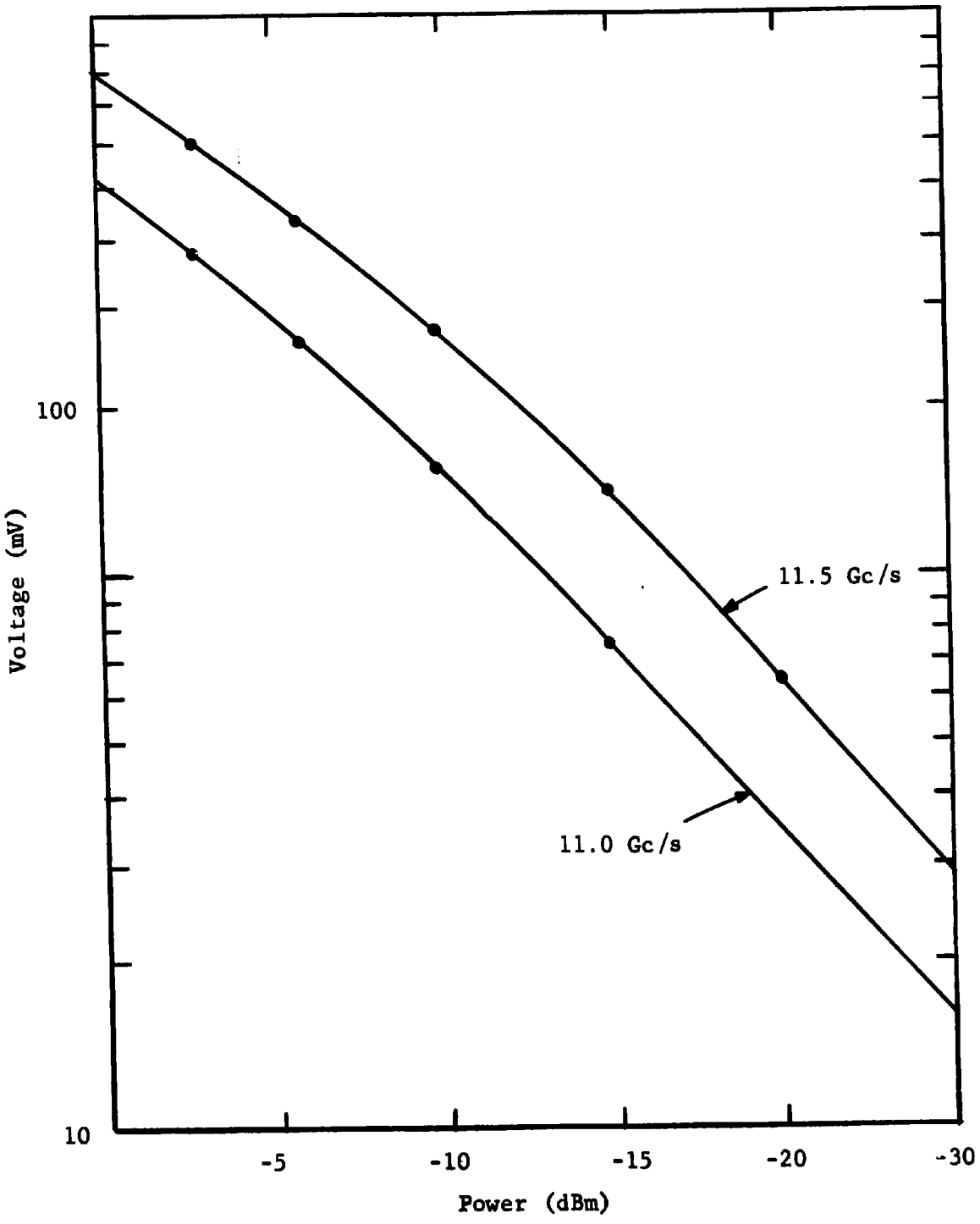

Figure 42 Detector Output Voltage Versus Input Power

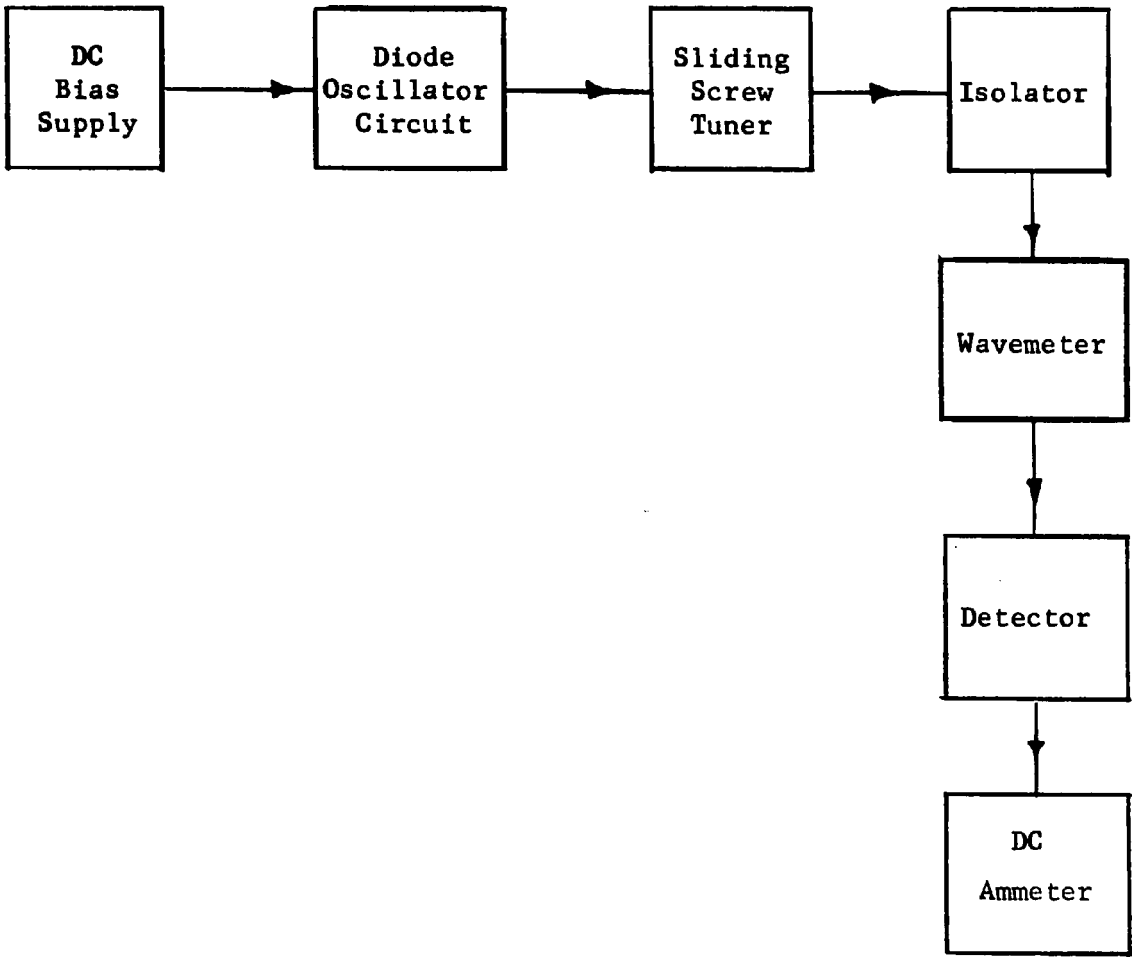

Figure 43 Oscillator Circuit for Life Tests

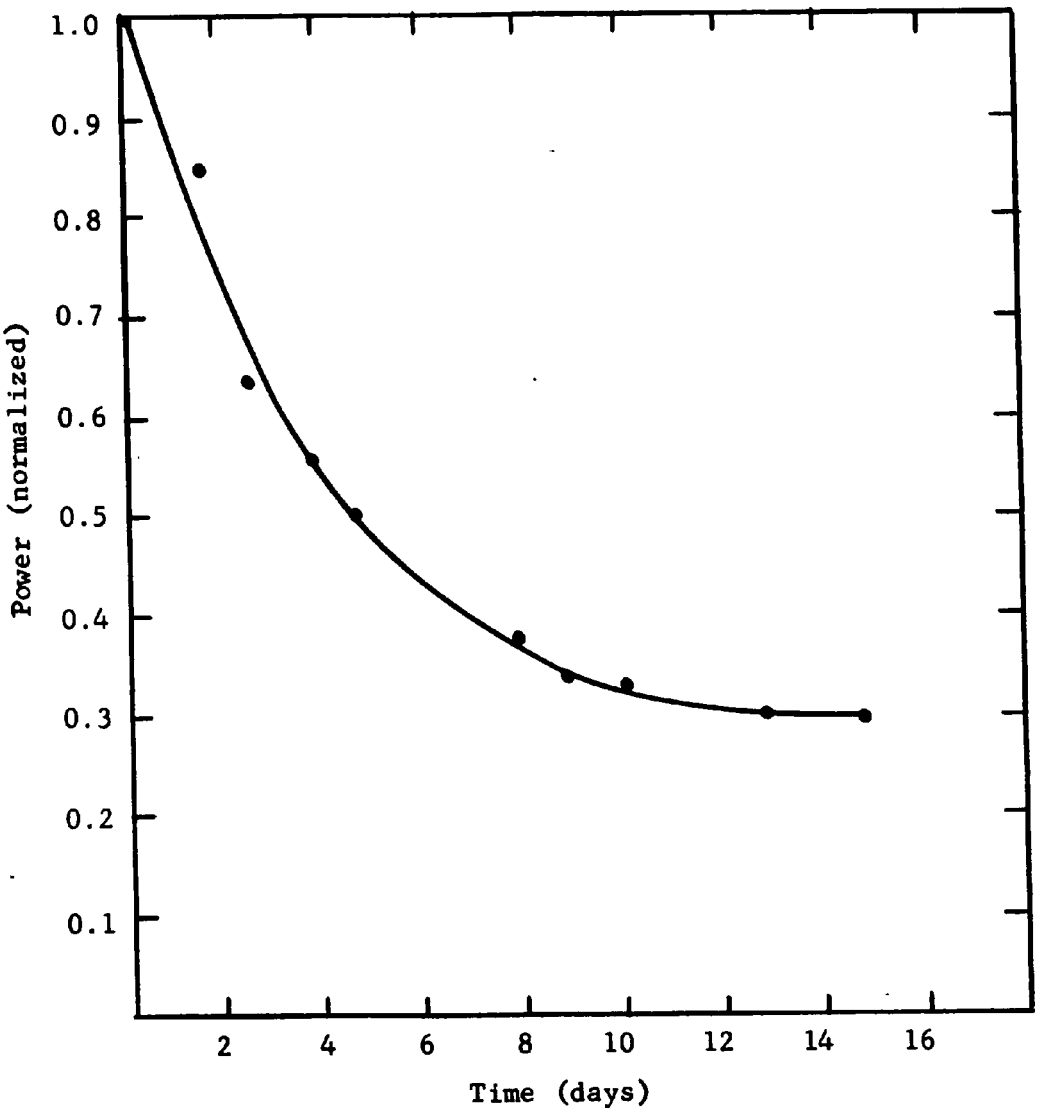

Figure 44 Oscillator Power Output Versus Time

CHAPTER V

RESULTS AND CONCLUSIONS

The maximum oscillator output power at the X-band frequencies was 630 μW at 10.8 Gc/s. This was obtained in the wafer circuit discussed earlier. The highest peak current diode to give fundamental oscillation at the X-band frequencies had a peak current of 21 mA. It was necessary to use a heavy forming pulse to obtain the high peak currents, and the peak current density for the X-band diodes was considerably less than the lower peak current diodes (less than 5 mA). Transmission resonance measurements on the X-band diodes showed a junction capacitance to peak current ratio of approximately 0.13 pF/mA. This was considerably higher than the ratio for the low peak diodes of 0.015 pF/mA. The power of 630 μW is probably close to the limit for the diodes presently available from the pulse alloy technique. However, superior diodes should be possible applying standard alloy techniques to the n-type GaAs similar to the p-type GaAs diodes made by Schneider (24). If the peak current density for large current diodes could be improved to match the low peak current diodes, one could expect almost an order of magnitude improvement in the output power.

The maximum oscillator power obtained at the millimeter frequencies was 200 μW at 50 Gc/s. This power output was obtained using the RG98/U wafer circuit discussed earlier. The 200 μW figure represents

the highest value from approximately 100 diodes. Several diodes gave output powers above 100 μW at frequencies between 45 Gc/s and 60 Gc/s in this circuit. The frequency of operation for individual diodes could be varied about 10 Gc/s by adjusting the tuning piston and the horizontal position of the diode, and still obtain output power within 3 dB of the maximum. Fundamental oscillations were obtained in this circuit for diodes with peak currents less than 5 mA. Output powers near the theoretical maximum were obtained for an appreciable number of diodes in this circuit, which implies that the horizontal positioning of thediode and the tuning piston are sufficient to optimize the load impedance seen by the diode. However, it was necessary to have the short circuiting piston very close to the diode. This distance was always less than a quarter wavelength, which caused the oscillation frequency to be below the self resonant frequency of the diode. If the piston was moved very far from the diode, the frequency of oscillation would drop to a frequency below the waveguide cutoff frequency of 40 Gc/s, and the only detectable output power was the second harmonic of this oscillation.

The ridge waveguide had a cutoff frequency less than 20 Gc/s, and it was possible to obtain fundamental oscillations with the piston far from the diode. Certain piston positions caused oscillation to cease, and the diodes could be stabilized. It would be possible to use this circuit with the diodes stabilized as reflection amplifiers at the millimeter frequencies.

A large number of the low peak current diodes were measured in the transmission resonance system to determine their equivalent circuit parameters. The diodes listed in Table 1 were measured in the 0.010 inch high

Table 1. Experimental Parameters of Low Peak Current Diodes

Diode	I_p (mA)	I_v (mA)	I_p/I_v -	R_- (ohms)	r_s (ohms)	C (pF)	R_-C (ps)	f_c (Gc/s)
1.	3.4	0.8	4.3	77	5.3	0.054	4.2	140
2.	2.8	0.7	4.0	95	5.4	0.043	4.1	160
3.	2.7	0.7	3.9	100	4.7	0.041	4.1	175
4.	3.2	0.9	3.6	87	5.2	0.051	4.4	148
5.	3.2	0.9	3.6	87	4.7	0.046	4.0	170
6.	5.5	1.4	3.9	50	4.5	0.054	2.7	188
7.	4.2	1.1	3.8	65	2.3	0.041	2.7	316
8.	3.5	0.9	3.9	77	3.5	0.049	3.8	193
9.	3.8	1.2	3.2	77	4.7	0.058	4.4	140
10.	4.2	1.3	3.2	69	4.2	0.044	3.0	205
11.	5.0	1.2	4.2	52	5.3	0.052	2.7	174
12.	4.9	1.1	4.5	52	4.5	0.065	3.4	155
13.	3.4	0.7	4.9	71	3.7	0.047	3.4	204
14.	4.0	1.2	3.3	71	3.3	0.062	4.4	164

RG98/U waveguide with the diodes in the center of the guide. The resulting data are fairly consistent, and can be fitted to the previously derived theoretical expressions. The first five diodes listed in the table are fairly consistent from several standpoints. The diodes have a narrow range of peak currents, and narrow range of peak to valley current ratios, and practically identical R_-C products. Experimentally, these diodes were all measured with the bias set at the valley point, which makes the measurement easier and more reliable. If the approximate equation relating peak current and resistive cutoff frequency is used,

$$I_p = \frac{K}{f_c^4} \tag{5-1}$$

it then becomes possible to take the experimental values of I_p and f_c for these diodes and compute the K for each diode and average. The result is

$$K = 2 \times 10^9 \tag{5-2}$$

for I_p measured in milliamperes

f_c measured in Gc/s.

This allows a prediction of the maximum possible power at a particular frequency using (3-51) and (3-52) of Chapter III. Also from the experimental results, the proper value for γ in (3-45) of Chapter III is 0.75. Further, the experimental value for ΔV for the n-type GaAs is about 400 millivolts. Substituting these numbers into (3-52), and using a frequency of 50 Gc/s, the power is

$$P_e = \frac{1}{3} \frac{3}{16} (400)(0.75) \frac{2 \times 10^9}{(3^{1/2}\ 50)^4} \ \mu W$$

$$= 670\ \mu W .$$

This is the absolute maximum power possible at this frequency and would

require diodes with peak currents around 35 mA. This is about 5 times larger than the peak currents of the diodes presently available. Another very difficult problem, if the high current diodes were available, is the circuit inductance and impedance. It would be necessary to reduce the inductance of the wire about one order of magnitude from the present value of 0.25×10^{-9} henries. This would be difficult, if not impossible, in a small waveguide structure, and it would be necessary to design another structure. Therefore, at the present time it appears that the wafer waveguide circuit is sufficient to optimize the diodes presently available.

From the experimental standpoint the 200 μW obtained represents the present maximum, and considerable circuit work would be necessary even if the diodes could be improved. Even then the increase in power would only be a factor of three. It is important to note that the experimental operation of the present diodes did not realize the maximum power at the maximum frequency derived in the theory. The experimental frequency of operation was about 25% of the resistive cutoff frequency, which means the efficiency was high, while the efficiency of the maximum power at the maximum frequency condition is only 33%. It would be interesting to realize the theoretical condition experimentally.

A more practical limit on the output power from a GaAs tunnel diode oscillator can be calculated for a high efficiency operation. A reasonable efficiency might be 85%. This requires the cutoff frequency f_c to be 3.33 times the frequency of the operation for (3-39) of Chapter III. If one assumes an operation frequency of 50 Gc/s, and uses (5-1) and (5-2), the power becomes:

$$P_e = (0.85)\left(\frac{3}{16}\right)(400)(5)(0.75)\ \mu W$$

$$= 240\ \mu W\ .$$

This is very close to the experimental value obtained, and is probably a very realistic limit. This theoretical limit and the maximum theoretical limit are plotted versus frequency in Figure 45.

A very important part of the experimental investigation for practical considerations was the electrical life of the millimeter frequency oscillators. Several oscillators were constructed in the wafer circuits, and were allowed to run continuously. The average time for the power output to fall 3 dB was approximately two days, and the power output was usually below the sensitivity of the detector in about one week. This severe degradation is contrary to the results of Schneider (24) with p-type GaAs at microwave frequencies, and will require further investigation. It is concluded from these investigations that while significant power can be obtained at millimeter frequencies from n-type GaAs tunnel diode oscillators, unless a significant improvement in the electrical lifetime is made, it shall be impossible to use these diodes for practical oscillators.

The relation for the available power as a function of frequency given by (5-1) applies to all point contact tunnel diodes, and shows explicitly how fast the power must be reduced as the operating frequency is increased.

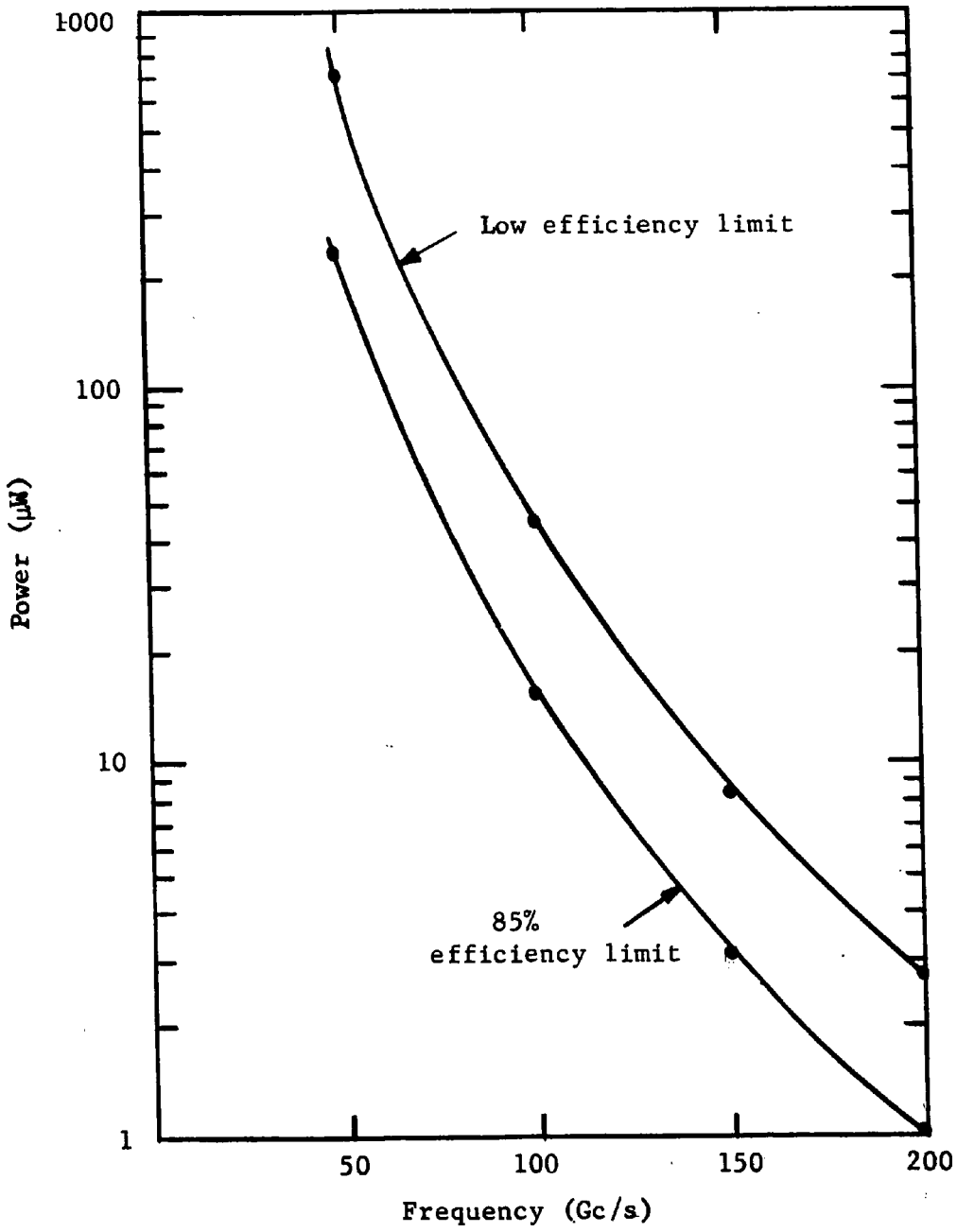

Figure 45 Power Output Limits Versus Frequency

LIST OF REFERENCES

1. Braun, F. A. and R. F. Trambarulo., unpublished work.

2. Bolinder, F., "Fourier Transforms in the Theory of Inhomogeneous Transmission Lines," Trans. of the Royal Inst. of Technology, Stockholm, Sweden, no. 48, 1951.

3. Burrus, C. A., "Millimeter Wave Esaki Diode Oscillators," Proc. IRE, vol. 48, p. 2024, December 1960.

4. Burrus, C. A., "Gallium Arsenide Esaki Diodes for High Frequency Applications," J. Appl. Phys., vol. 32, pp. 1031-1036, June 1961.

5. Burrus, C. A., "Backward Diodes for Low-Level Millimeter-Wave Detectors," IRE Trans. on Microwave Theory and Techniques, vol. MTT-11, p. 357, 1963.

6. Chynoweth, A. G., unpublished work.

7. Cunningham, W. J., Nonlinear Analysis, McGraw-Hill, 1958, pp. 140-151.

8. DeLoach, B. C., "A New Microwave Measurement to Characterize Diodes, and an 800 Gc Cutoff Frequency Varactor Diode at Zero Volts Bias," IEEE Trans. on Microwave Theory and Techniques, vol. MTT-12, pp. 15-20, January 1964.

9. Eng, S. T., "Low-Noise Properties of Microwave Backward Diodes," IRE Trans. on Microwave Theory and Techniques, vol. MTT-9, pp. 419-425, September 1961.

10. Esaki, L., "New Phenomena in Narrow Ge P-N Junctions," Phys. Rev., vol. 109, p. 603, 1958.

11. Hall, R. N., "Tunnel Diodes," IRE Trans. on Electron Devices, vol. ED-7, pp. 1-9, January 1960.

12. Hines, M. E., "High-Frequency Negative-Resistance Circuit Principles for Esaki Diode Applications," BSTJ, vol. 39, p. 477, March 1960.

13. Jeans, J. H., The Mathematical Theory of Electricity and Magnetism, Cambridge University Press, 1915.

14. Kane, E. O., "Theory of Tunnelling," J. Appl. Phys., vol. 32, p. 83, 1961.

15. Kim, C. S. and A Brandli, "High-Frequency High-Power Operation of Tunnel Diodes," IRE Trans. on Circuit Theory, vol. CT-8, p. 416, December 1961.

16. Lesk, I. A., et al., "Germanium and Silicon Tunnel Diodes: Design, Operation, and Application," IRE WESCON Conv. Rec., pt. 3, pp. 9-31, 1959.

17. Lindmayer, J. and C. Y. Wrigley, Fundamentals of Semiconductor Devices, Van Nostrand, 1965, pp. 42-47.

18. Montgomery, C. G., E. M. Purcell, and R. H. Dicke, Principles of Microwave Circuits, McGraw-Hill, 1948, pp. 30-37.

19. Nanavanti, R. P., Introduction to Semiconductor Electronics, McGraw-Hill, 1963, pp. 108-115.

20. Oguey, H. J., "Analysis of the Frequency and Power Performance of Tunnel Diode Generators," IEEE Trans. on Microwave Theory and Techniques, vol. MTT-12, pp. 412-419, September 1963.

21. Pucel, R. A., "Physical Principles of the Esaki Diode and Some of Its Properties as a Circuit Element," Solid-State Electronics, vol. 1, pp. 22-23, 1960.

22. Schelkunoff, S. A., "The Impedance Concept and Its Application to Problems of Reflection, Refraction, Shielding, and Power Absorption," BSTJ, vol. 17, p. 17, 1938.

23. Schelkunoff, S. A., Electromagnetic Waves, Van Nostrand, 143, p. 494.

24. Schneider, M. V., "A 5-Gc Tunnel Diode Oscillator with 9-Milliwatt Output from a Single Diode," BSTJ, vol. 42, pp. 2972-2974, November 1963.

25. Schuller, M. and W. W. Gartner, "Large-Signal Circuit Theory for Negative-Resistance Diodes, in Particular Tunnel Diodes," Proc. IRE, vol. 49, pp. 1268-1278, August 1961.

26. Sharpless, W. M., "High-Frequency Gallium Arsenide Point-Contact Rectifiers," BSTJ, vol. 38, pp. 259-270, January 1959.

27. Sharpless, W. M., "Point-Contact Wafer Diodes for Use in the 90 to 140 Gc Frequency Range," BSTJ, vol. 42, pp. 2496-2499, September 1963.

28. Sharpless, W. M., "A Calorimeter for Power Measurements at Millimeter Wavelengths," IRE Trans. on Microwave Theory and Techniques, vol. MTT-2, pp. 45-47, September 1954.

29. Slater, J. C., Microwave Transmission, McGraw-Hill, 1942, pp. 288-296.

30. Smythe, W. R., Static and Dynamic Electricity, McGraw-Hill, 1939, p. 451.

31. Stratton, J. A., Electromagnetic Theory, McGraw-Hill, 1941, p. 15.

32. Southworth, G. C., Principles and Applications of Waveguide Transmission, Van Nostrand, 1950, p. 104.

33. Trambarulo, R. F. and C. A. Burrus, "Esaki Diode Oscillators from 3 to 40 Gc," Proc. IRE, vol. 48, p. 1776, October 1960.

34. Trambarulo, R. F., "Esaki Diode Amplifiers at 7, 11, and 26 Gc," Proc. IRE, vol. 48, p. 2022, December 1960.

35. Trambarulo, R. F., "Some X-Band Microwave Esaki-Diode Circuits," presented at 1961 International Solid-State Circuits Conference, Philadelphia, Pa., February 1961.

36. Van der Zeil, A., Solid State Physical Electronics, Prentice-Hall, 1957, p. 277.

37. Vieland, L. J. and I. Kudman, "Behavior of Selenium in Gallium Arsenide," J. Phys. Chem. Solids, vol. 24, pp. 437-441, March 1963.

38. Yariv, A., J. S. Cook, and P. Butzien, "Operation of an Esaki Diode Microwave Amplifier," Proc. IRE, vol. 48, p. 1155, June 1960.

39. Young, D. T., C. A. Burrus, and R. C. Shaw, "High Efficiency Millimeter Wave Tunnel Diode Oscillators," Proc. IEEE, vol. 52, p. 1260, October 1964.

40. Zener, C., Proc. Royal Soc. (London), vol. 145, p. 523, 1934.